PLOS ONE

RESEARCH ARTICLE

Anticryptosporidial action mechanisms of *Launaea spinosa* extracts in *Cryptosporidium parvum* experimentally infected mice in relation to its UHPLC-MS metabolite profile and biochemometric tools

Mai M. Elghonemy[1☯], Mohamed G. Sharaf El-Din[2☯], Dina Aboelsoued[3☯], Mohamed F. Abdelhameed[4], Mohamed A. El-Saied[5], Nagwa I. Toaleb[3], Mohamed A. Farag[6]*, Abdelsamed I. Elshamy[1]*, Abdelbaset M. Elgamal[7]

1 Department of Natural Compounds Chemistry, National Research Centre, Giza, Egypt, **2** Pharmacognosy Department, Faculty of Pharmacy, Port Said University, Port Said, Egypt, **3** Parasitology and Animal Diseases Department, Veterinary Research Institute, National Research Centre, Giza, Egypt, **4** Pharmacology Department, Medical Research and Clinical Studies Institute, National Research Centre, Giza, Egypt, **5** Department of Pathology, Faculty of Veterinary Medicine, Cairo University, Giza, Egypt, **6** Pharmacognosy Department, Faculty of Pharmacy, Cairo University, Cairo, Egypt, **7** Department of Chemistry of Microbial and Natural Products, National Research Centre, Giza, Egypt

☯ Equal contribution
* elshamynrc@yahoo.com (AIE); mohamed.farag@pharma.cu.edu.eg (MAF)

OPEN ACCESS

Citation: Elghonemy MM, Sharaf El-Din MG, Aboelsoued D, Abdelhameed MF, El-Saied MA, Toaleb NI, et al. (2025) Anticryptosporidial action mechanisms of Launaea spinosa extracts in *Cryptosporidium parvum* experimentally infected mice in relation to its UHPLC-MS metabolite profile and biochemometric tools. PLoS ONE 20(3): e0317497. https://doi.org/10.1371/journal.pone.0317497

Editor: Horacio Bach, University of British Columbia, CANADA

Received: July 10, 2024

Accepted: December 30, 2024

Published: March 3, 2025

Data availability statement: All relevant data are within the paper and its Supporting Information files.

Funding: The author(s) received no specific funding for this work.

Abstract

Background

Cryptosporidium parvum, a leading cause of diarrhea, is responsible for millions of food and waterborne illnesses in humans and animals worldwide. *Launaea spinosa* (Asteraceae family) is a common herb found in the desert of the Mediterranean region, encompassing the peninsula of Sinai. Traditionally, it has been utilized for managing gastrointestinal issues and inflammation.

Methods and findings

The present study aimed to assess *Launaea spinosa* (LS) extracts viz. ethyl acetate (LS-EtOAc), ethanol (LS-EtOH), and *n*-butanol (LS-BuOH), of different polarities against *C. parvum* in experimentally infected mice based on immunological, biochemical, histo- and immunohistochemical assays. Extracts were characterized via UHPLC-ESI-LIT-Orbitrap-MS and metabolite profiles were subjected to correlation modeling with bioactivities *via* supervised Partial Least Square (PLS) to identify active agents. Most *L. spinosa* extracts reduced fecal *C. parvum* oocyst count and mucosal burden ($P < 0.05$) than untreated infected mice, with LS-BuOH (200 mg/kg) exerting the highest reduction percentage (97%). These extracts increased immunoglobulin G (IgG) levels in infected and treated mice at all examined days post treatment. Also, the highest Interferon-Gamma (IFN-γ) and Interleukin-15 (IL-15) levels were obtained after 10 days of post inoculation

Competing interests: There is no conflict of interest.

(dPI), which were restored to a healthy state after 21 days, concurrent with a decrease in Tumor Necrosis Factor-Alpha (TNF-α) ($P < 0.001$). The increased liver enzyme (alanine aminotransferase, aspartate aminotransferase, and alkaline phosphatase) levels with infection were likewise reduced with extract administration. The LS extracts caused a significant increase in antioxidant glutathione peroxidase (GSH-Px) and catalase ($P < 0.001$). Examination of colon tissue revealed that infected-treated mice with LS extracts exhibited a reduction in the expression of cleaved caspase-3, damage score, and degenerative changes. Metabolite profiling of different *L. spinosa* extracts led to the identification of 86 components, primarily phenolic acids, flavonoids, triterpenoid saponins, and fatty acids, with the first report of sulfated triterpenoid saponins in *Launaea* genus. PLS regression analysis revealed that bioeffects were significantly positioned close to LS-BuOH extract (R^2: 0.9) mostly attributed to triterpenoid saponins and flavonoid glycosides.

Conclusions

This study demonstrated potential anti-cryptosporidial effects of LS extracts, especially LS-BuOH, suggesting its potential for inclusion in future nutraceuticals aimed at *C. parvum* treatment.

1. Introduction

Cryptosporidium is a zoonotic intracellular protozoan parasite which is one of the major contributors to diarrhea in humans and animals [1,2]. It is considered the main cause of waterborne disease outbreaks worldwide [3] and is responsible for more than eight million foodborne disease cases annually worldwide [4]. In livestock animals, *Cryptosporidium* infection varies depending on animal species, geographical area, rearing practices, and the diagnostic tools used [5]. It is more frequent in neonate and young calves, with severity depending on age, calf immunity, dose of infection, geographical distribution, season, and mixed infection with other pathogens [6]. *Cryptosporidium parvum* (*C. parvum*) is widely spread in cattle herds causing significant economic losses, high morbidity, growth retardation, high treatment costs and representing a dominant cause of calf scours [5,7]. Currently, no prophylactic, therapeutic or natural products are fully effective against *C. parvum* infection either in humans or animals [8]. Consequently, there is increasing interest in identifying new therapeutics [9]. Many therapeutic agents have been tested for the treatment of cryptosporidiosis either *in vitro* or *in vivo,* albeit with limited effect [10]. Few have shown efficacy in reducing *C. parvum* oocyst shedding and reducing the severity and duration of diarrhea [11].

Numerous therapeutic and pharmacological uses of medicinal plants and their bioactive byproducts are well known. Across the world, *Launaea* Cass. (Family Asteraceae) is a common genus, particularly in Africa, the South Mediterranean, and Asia, with ca. 54 species [12]. *Launaea* plants exhibit traditional uses worldwide including the treatment of gastrointestinal illnesses, inflammation, wounds, fever, diarrhea, and infections of the stomach, breast, liver, skin, and infections of insects [12,13]. Biological assays have also verified the antibacterial, antioxidant, hypoglycemic, insecticide, cancer prevention, fungicide, anti-inflammatory, and anti-angiogenic capabilities of several *Launaea* species extracts and/or their isolated compounds [13–15]. *L. spinosa* (Forssk.) Sch. Bip. ex Kuntze is commonly found in the desert regions of Palestine, Jordan, Egypt (Sinai), and northwest Saudi Arabia [16]. It has traditionally been employed to treat fever, pain, wounds, skin diseases, gastrointestinal problems and inflammation [17]. The health advantages of L. spinosa are mediated through its

phytochemical components such as flavonoids, coumarins, sesquiterpenes, and essential oils [12,18,19].

The current study was conducted with the following objectives: (i) assess the anti-parasitic action mechanism of *L. spinosa* extracts of varying polarities, ethyl acetate (EtOAc), hydro-ethanol (EtOH), and *n*-butanol (BuOH), against molecularly identified *Cryptosporidium parvum* in experimentally infected mice; (ii) identify bioactive metabolites in extracts of varying composition; and (iii) illustrate the relationship between bioactivities and extracts' identified metabolites using biochemometric tools, such as partial least square (PLS).

2. Materials and methods

2.1. Plant material and extracts preparation

Aerial parts of *L. spinosa* were collected from Wadi Hagul, in the Egyptian Eastern Sahara (30°02′34.3° N, 32°05′40.6° E) during the flowering stage in May 2022. The Plant Ecology Professor at Mansoura University, Dr. Ahmed M. Abd-ElGawad, authenticated and verified the species and the voucher specimen, Mans. 001121905, was placed in the Faculty of Science` herbarium of Mansoura University.

Collected *L. spinosa* aerial parts were cleaned first from dirt and then left in an open, fully dry, and shady area for 21 days, until they were completely dry. The dried plant material was finely powdered using a clean plant grinder. Three equally weighed portions (500 g each) were randomly aliquoted from the 1.5 kg of powdered aerial dried parts of *L. spinosa* to be subjected for 5 days to the different extraction solvents. Ethyl acetate (EtOAc, 2L), 70% hydro-ethanol (EtOH, 2L), and *n*-butanol (*n*-BuOH, 2L) were used to extract each part separately. After filtration, the solvent was evaporated under reduced pressure using a rotavapor at 45–50 °C to yield three separated black residues weighing 17.8, 22.3, and 19.2 g, respectively. Extracts were kept in three opaque glass vials at a temperature of –4 °C until further assays or analysis.

2.2. Biological assaying

2.2.1. Ethical approval. All animal experimental procedures were performed at the National Research Centre (NRC) Animal House and Immunology and Parasitology Laboratory, Veterinary Research Institute, NRC. All methods and experiments were performed in accordance with the relevant guidelines and regulations of the International Animal Ethics Committee guidelines and the Institutional Guidelines of the National Research Centre Animal Research Committee (Approved Protocol No. 8444052023) and in accordance with ARRIVE guidelines.

2.2.2. Isolation and identification of *Cryptosporidium* oocysts. Fecal samples were collected from 20 diarrheic newborn buffalo calves (aged 10–20 days) reared by local farmers in Giza Governorate, Egypt, from the calves' rectum using sterile latex gloves in separate clean labeled containers. The collected samples were transported to Immunology and Parasitology Lab, NRC, at the day of collection, then prepared and stained with modified Ziehl-Neelsen (MZN) staining [20] and Carbol fuchsin [21], and then examined under a light microscope (LEICA Imaging Systems Ltd., England) with oil immersion at the day of collection. *Cryptosporidium* oocysts were concentrated using Sheather's sugar solution floatation method [22]. Oocysts were collected and stored at 4°C in a 2.5% potassium dichromate solution ($K_2Cr_2O_7$, Sigma-Aldrich, Canada). Genomic DNA was extracted from 10 isolated oocyst samples using a DNA extraction Kit (GeneDireX Inc., USA) according to the manufacturer's protocol, and DNA concentration was measured by a microvolume spectrophotometer (Q9000, Quawell, USA) and stored at – 20°C until further analysis. For *Cryptosporidium* sp. identification, amplification of the extracted DNA

was performed using PCR targeting *Cryptosporidium* oocyst wall protein (COWP) gene, 553 bp, (Cry9: Forward 5′-GGACTGAAATACAGGCATTATCTTG-3′ and Cry15: Reverse 5′- GTAGATAATGGAAGAGATTGTG-3′) according to Feltus [23] using a thermal Cycler (BIO-RAD, Singapore). PCR products were visualized using Molecular Imager (BIO-RAD, Singapore) in 1.5% Agarose gel electrophoresis stained with RedSafe (Intron Biotechnology, Republic of Korea), and estimated for band size with a 100 bp ladder (QIAGEN, USA).

Cryptosporidium-positive PCR products were purified using Gel Extraction Kit (Qiagen, USA) following the manufacturer's instructions. Purified products were sequenced with Big Dye Terminator V3.1 Cycle Sequencing Kit (Perkin-Elmer, USA) using an automated sequencer (ABI 3130, Applied Biosystems, USA). The resulting sequences were corrected by ChromasPro 1.7 software (Technelysium Pty Ltd., Australia) and then compared with those available in GenBank using nucleotide BLAST (https://blast.ncbi.nlm.nih.gov/Blast.cgi) and submitted in GenBank. Multiple sequence alignment was performed as designed by Thompson [24] using CLUSTAL W 1.83 of MegAlign module of Lasergene DNAStar software Pairwise. Phylogenetic analysis was performed with maximum likelihood, neighbor-joining and maximum parsimony in MEGA6 software [25].

2.2.3. Antigen and hyperimmune serum assay. Infective *C. parvum* oocysts (identified previously by PCR) were pooled from corresponding oocyst inoculums, washed 3 times with Phosphate Buffered Saline (PBS) solution (pH = 7.2), counted by a hemocytometer, and diluted in double distilled water to obtain infection dose 10^5 oocysts/mL [26]. Ten parasite-free Swiss albino mice, 3 weeks old, obtained and housed in good conditions at specific cages at the Animal House, NRC, Egypt, with free access to food and water, were infected orally using gastric tubes 1 h before meal by 10^5 *C. parvum* oocysts in 250 μL PBS solution (pH = 7.2). After four days, mice fecal pellets were collected daily for 3 weeks, and examined with MZN staining [20]. Oocysts in fecal pellets were isolated by Sheather's sugar solution. *C. parvum* antigen was prepared from isolated oocysts according to Kaushik et al., 2009 [27] using Vibra Cell VCX750 Sonicator (Sonics & Materials, USA). Then, antigen protein content was estimated by Lowry's method [28] and stored at –20 ºC until use.

Hyperimmune serum was prepared by immunization of 2 parasite-free rabbits, housed in good conditions at specific cages at the Animal House, NRC, Egypt, with free access to food and water, using 40 μg/Kg *C. parvum* antigen according to Fagbemi [29]. After immunization, blood samples were collected from the rabbits' ear vein as described by Aboelsoued [30]. Serum was separated by centrifugation and stored at –20 ºC for further use.

2.2.4. Affinity purification of *C. parvum* antigen. The rabbit hyperimmune serum was defrosted and dialyzed for three days in a coupling buffer (0.1 M $NaHCO_3$, 0.5 M NaCl, pH = 8.4) and then coupled to 2 mg/mL-swollen beads of cyanogen bromide-activated Sepharose-4B (CNBr Sepharose-4B, Sigma-Aldrich, USA). The prepared *C. parvum* antigen was applied to the affinity column (Flex-Column, Kimble, USA) as described by Aboelsoued et al. [8]. The protein content of the purified antigen was estimated as described by Lowry's method [28] and then stored at –20 ºC for further use.

2.2.5. Experimental design of the *L. spinosa* extracts` inhibitory effects against *C. parvum*. Forty-five mice were randomly divided into nine groups (five mice/ each). **Group 1**: Control negative group (uninfected-untreated). **Group 2**: Control positive group, mice were infected orally using gastric tubes 1 h before meal by $1x10^5$ *C. parvum* oocysts in 250 μL PBS solution (pH = 7.2) [26]. **Group 3**: Mice were infected by *C. parvum* oocysts and treated with 100 mg Nitazoxanide as a reference drug. **Group 4**: Mice were infected by *C. parvum* oocysts and treated with 100 mg/Kg of *L. spinosa* ethyl acetate extract (LS-EtOAc). **Group 5**: Mice were infected by *C. parvum* oocysts and treated with 200 mg/Kg of LS-EtOAc. **Group 6**: Mice were infected by *C. parvum* oocysts and treated with 100 mg/Kg of *L. spinosa* ethanol extract

(LS-EtOH). **Group 7**: Mice were infected by *C. parvum* oocysts and treated with 200 mg/Kg of LS-EtOH. **Group 8**: Mice were infected by *C. parvum* oocysts and treated with 100 mg/Kg of *L. spinosa* butanol extract (LS-BuOH). **Group 9**: Mice were infected by *C. parvum* oocysts and treated with 200 mg/Kg of LS-BuOH.

All animals from Group 3 through Group 9 received oral treatments as described above once per day for 3 days starting from the third day of inoculation (after oocysts appeared in mice feces). After inoculation, all mice were observed for three weeks. About 200 μL of blood was collected from the retro-orbital sinus of each mouse using a sterile hematocrit capillary tube along the inner corner of the eye twice per week from all groups. Sera were separated and stored at –20 ºC for further use. At the end of experiment, all mice were sacrificed gently and rapidly by cervical dislocation under anesthesia using intraperitoneal injection of Sodium pentobarbital at dose of 40 to 50 mg/Kg and then disposed according to the Safety and Health Committee of the National Research Centre (NRC). Small intestines were collected and rinsed free of intestinal content and then cut in two sequential fragments taken from the ileum; one fragment was used for histopathological and immunohistochemical examination, and the other was used for mucosal *C. parvum* oocysts and developmental stages count detection by MZN staining. Bedding was changed every day and fecal samples were collected daily starting from the third day post inoculation (dPI) until the end of the experiment.

2.2.6. Fecal oocysts' shedding. Fecal pellets were collected daily from all mice groups for the determination of the number of *C. parvum* oocysts output counted from each group. Each fecal sample was smeared on a glass slide, stained according to MZN [20]. The number of oocysts were counted in 50 microscopic fields (100X objective) [31]. Fecal pellets were collected from the uninfected mice group parallel to the infected groups and examined to confirm their negativity during the experiment. Percent of reduction (PR), representing the decrease in oocysts' count of treated mice groups than the infected-untreated mice group, was calculated according to **Farid** [32] using the following formula:

$$\text{Percent of reduction (PR)} = \frac{\text{No. of oocysts in infected untreated group} - \text{No. of oocysts in infected treated group}}{\text{No. of oocysts in infected untreated roup}} \text{X100}$$

2.2.7. Quantification of mucosal burden. At the 10th day post inoculation (peak of oocyst shedding in infected untreated mice), two mice were sacrificed from each infected group for quantification of mucosal burden. Small intestine fragments taken from the ileum were cleaned free of intestinal content and homogenized in 10 volumes of PBS solution. Ten microliters of homogenate were smeared onto a glass slide then stained according to MZN [20]. Oocysts and developmental stages were counted on the whole slide and results were expressed as oocysts' number/ mg of tissue.

2.2.8. C. parvum specific antibodies detection. Specific *C. parvum* Immunoglobulin G (IgG) titer in infected mice serum after infection and treatments at different intervals (0-day, 5 days post treatment (dPT), 10 dPT and 15 dPT) was monitored using indirect ELISA from the purified fraction isolated from *C. parvum* oocyst antigen as previously described by Priest [33]. Optical densities (OD) of the developed color were recorded at 450 nm using automated microplate ELISA reader (ELx800UV, BioTek, USA). Concentrations of the used antigen, sera and conjugates' dilutions were calculated by checkerboard titration. Cut-off value was estimated by mean OD values of negative sera + 3 standard deviation (SD).

2.2.9. Cytokine levels. Using Sandwich ELISA kits, IFN-γ, IL-15 (Sunlong Biotech, China), and TNF-α (Sigma-Aldrich, Saint Louis, USA) levels were assessed in mice sera as described by the manufacturer. Optical density was measured using automated microplate

ELISA reader (ELx800UV, BioTek, USA) at 450 nm. Concentrations were estimated using standard curves performed at the same assays.

2.2.10. Biochemical marker assays. Liver enzymes including alanine aminotransferase (ALT), aspartate aminotransferase (AST), alkaline phosphatase (ALP), and antioxidant parameters: glutathione peroxidase (GSH-Px) and catalase were determined using colorimetric method according to manufacturer using kits (Biodiagnostic, Giza, Egypt). The colorimetric reaction was measured using UV-Visible spectrophotometer (Cary 100, Agilent Technologies, Inc., Australia).

2.2.11. Histopathological examination of intestines from different experimental groups. Intestinal specimens from each animal among experimental groups were collected and well-preserved in 10% neutral buffered formalin then routinely processed in alcohol followed by xylene and embedded in blocks of paraffin that sectioned at 5 μm in thickness, stained with hematoxylin and eosin (H&E) and examined under light microscope (Olympus BX43) connected to digital camera (Olympus DP27) with CellSens dimensions software (Olympus, Tokyo, Japan). The assessment of histopathological alternations was quantified in five random microscopical fields from each animal and scored from (0–3) as follows: (0) means no changes, (1) means mild change, (2) means moderate changes and (3) means severe changes. Concisely, the histopathological alterations were assigned for five parameters (mucosal apoptosis and necrosis, infiltration of inflammatory cells, congestion, mucosal edema, apoptosis, and necrosis of glandular epithelium). The total histopathological lesion score was obtained with summation of the five parameters evaluated altogether [34].

2.2.12. Immunohistochemical expression of Cleaved Caspase-3. The expression level of cleaved caspase-3 in the intestinal segment was analyzed using primary antibodies against caspase-3 (diluted 1:100; ab32042, Abcam) that were incubated overnight at 4˚C. The corresponding secondary antibody used was horseradish peroxidase (HRP)-labeled goat anti-mouse antibody (Abcam) by incubation for 2 h, after which diaminobenzidine tetrachloride (DAB, ThermoScientific) was used to visualize the immune reaction. The positive expression level was determined as a brown color that was assessed as area % using Olympus CellSens dimensions software (Olympus, Tokyo, Japan) [35].

2.3. Metabolites profiling of *L. spinosa* extracts *via* high-resolution ultra-performance liquid chromatography-mass spectrometry analysis (UHPLC-ESI-LIT-Orbitrap-MS)

The three *L. spinosa* extracts' UHPLC-ESI-LIT-Orbitrap-MS analyses were performed under the same reported methodology and conditions in **Farrag** et al [36] and **Abdel Shakour** et al [37]. The analysis of the three *L. spinosa* extracts was conducted using both negative and positive modes of electrospray ionization (ESI) to achieve a comprehensive metabolome profile. The negative ionization mode demonstrated superior sensitivity, producing pronounced $[M-H]^-$ ions and achieving higher signal-to-noise ratios with less background noise compared to the positive ionization mode. The identification of metabolites relied on several criteria: order of elution, ultraviolet-visible (UV/Vis) spectroscopy, molecular formulas predicted using high-resolution mass spectrometry (HR-MS), fragmentation patterns in tandem MS-MS, matching with known standards, and comparison against a proprietary database and Mass Bank (https://massbank.jp/) as well as the Dictionary of Natural Products (DNP, 2015).

2.4. Statistical analysis

Statistical analyses were performed with SPSS 19.0 for Windows (SPSS, Inc., USA) and values were given as Means ± Standard Error. Data were tested for normality via

Kolmogorov-Smirnov test of normality. A one-way analysis of variance (ANOVA) was conducted, followed by Tukey's multiple comparisons test, to assess the statistical significance of variations among groups in terms of oocyst counts in fecal pellets and mucosal tissue, concentrations of ELISA, cytokines, and biochemical parameters. The non-parametric data of lesion score was compared by Kruskal-Wallis and Dunn's multiple comparisons test. Significant differences were considered when $P < 0.05$.

3. Results

3.1. Biological results

3.1.1. PCR and phylogenic analysis. DNA of *Cryptosporidium* sp. was detected in fecal samples of 10 out of 20 diarrheic newborn buffalo calves (50%) using the COWP gene. After sequencing and phylogenic analysis, *C. parvum* isolate (GenBank: OQ121955.1) was identified being 100% (495/495) identical to those of *C. parvum* detected in buffaloes from Egypt (GenBank: ON730708.1 and ON730707.1). Phylogenetic analysis revealed that this genotype was clustered in a well-supported branch with other *C. parvum* sequences (**Fig 1**).

3.1.2. Fecal oocysts' shedding. Examination of mice fecal smears to detect *C. parvum* oocysts revealed that mice shed many oocysts from the 3rd dPI and there was a gradual decrease in *C. parvum* oocysts' shedding in the infected-untreated mice from the 10th dPI which continued to decrease until no oocysts were detected in day 20 PI. In parallel, *C. parvum* oocyst counts in all infected and treated groups showed decline in LS-BuOH, LS-EtOH, NTZ, and LS-EtOAc from the 5th, 6th, 8th, 9th dPI, respectively. There was a statistically significant difference ($P < 0.05$) between oocysts shedding in infected-untreated, *L. spinosa*-treated and NTZ-treated groups until reaching negligible oocyst counts or no oocysts. The LS-BuOH extract reduced *C. parvum* oocysts' count significantly ($P < 0.05$) in experimentally infected mice than other *L. spinosa* extracts and NTZ treatments in almost all day's PI (**Table 1**). Interestingly, *C. parvum* oocysts in fecal pellets of LS-BuOH treated mice appeared deformed in shape, lacking inner structure, as compared to infected-untreated and other treated mice fecal pellets (**Fig 2**).

Regarding oocysts' shedding reduction after 10 days of infection in the infected and treated mice groups, LS-BuOH extract 200 mg/Kg showed the strongest reduction (97%) between the experimental groups (Fig 3). At the 21st dPI, almost all groups reached 100% oocyst reduction except in the case of NTZ and LS-EtOAc extract 100 mg/Kg treated groups (**Fig 3**).

3.1.3. Mucosal burden. Oocysts and developmental stages enumerated in mucosal tissue of infected-untreated mice exhibited the highest number after 10- and 21-dPI. Both concentrations of LS-BuOH extract (200 mg/Kg and 100 mg/Kg) showed the strongest significant anti-cryptosporidial effect ($P < 0.05$) on *C. parvum* oocysts' mucosal burden (**Table 2**), and in agreement with fecal oocysts' shedding PR shown in **Fig 3**.

3.1.4. The humoral immune response of healthy, infected, and treated mice. Levels of specific *C. parvum* antibodies IgG showed a significant increase in the infected and treated mice ($P < 0.05$) at all dPT as follows: 1 dPT (5th dPI), 6 dPT (10th dPI), 11dPT (15th dPI), 17 dPT (21st dPI), compared to infected-untreated mice. IgG levels increased gradually from the first dPT with highest level detected at 17 dPT in mice from group 5 treated with 100 and 200 mg/Kg LS-BuOH extract at an OD value of 0.885 and 0.769, respectively, as compared with other *L. spinosa* extracts treated groups (**Fig 4**).

3.1.5. Cytokines profile. The levels of serum cytokines including IFN-γ, IL-15 and TNF-α were significantly ($P < 0.001$) higher in serum of *C. parvum* experimentally infected-untreated mice group after 10 and 21 dPI compared to the control healthy rats (**Table 3**). Treatment of mice by Nitazoxanide and *L. spinosa* ethyl acetate and ethanol extracts showed significantly ($P < 0.001$) lower IFN-γ levels compared to the infected-untreated mice.

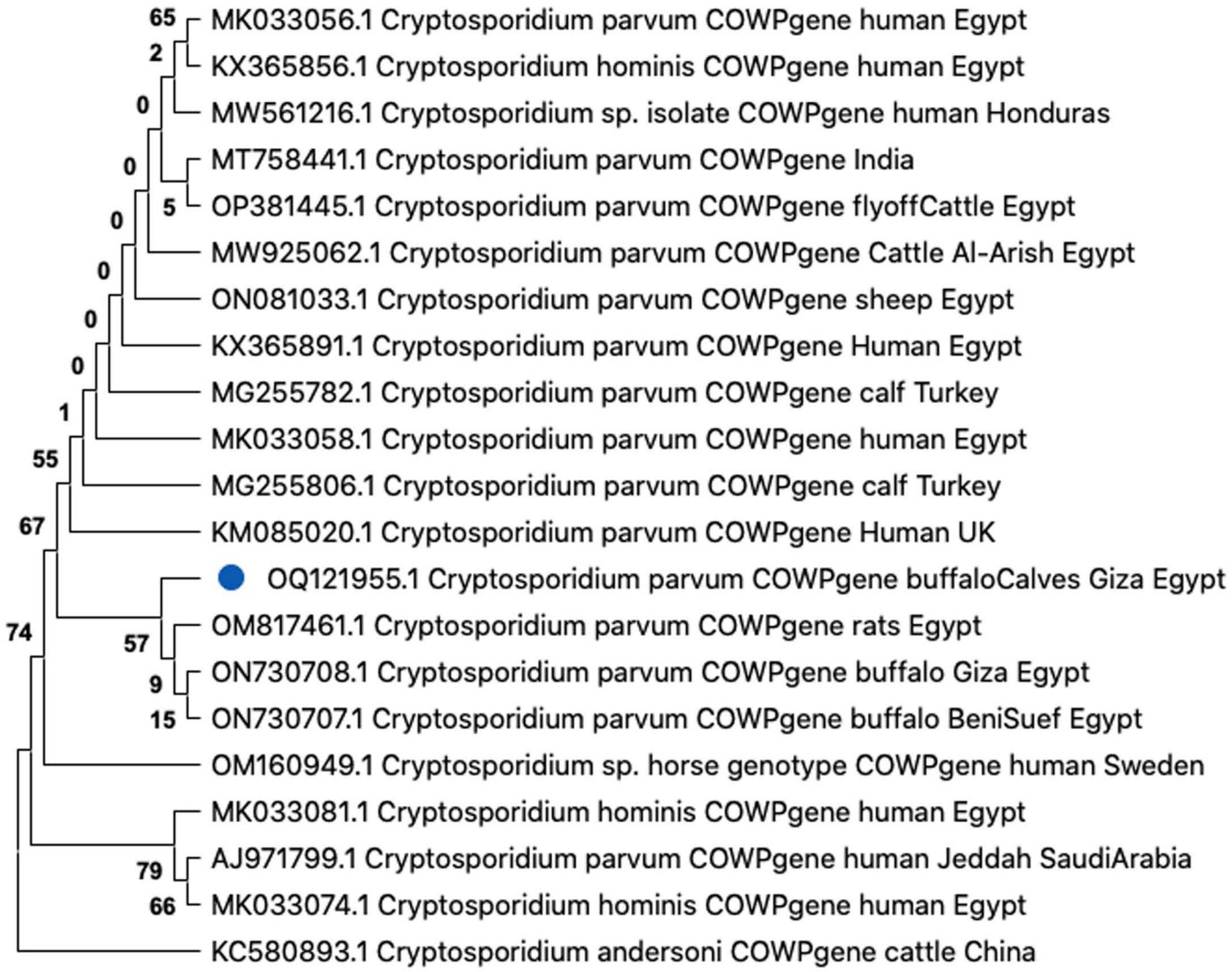

Fig 1. Phylogenetic tree based on the maximum likelihood method using *Cryptosporidium* oocyst wall protein (COWP) gene for *Cryptosporidium* spp. The obtained sequence is highlighted (blue dot).

https://doi.org/10.1371/journal.pone.0317497.g001

In contrast, the LS-BuOH extract group showed significantly ($P < 0.001$) higher levels of IFN-γ after 10 dPI at a dose of 100 mg/Kg (195.92 ± 1.77 ng/mL) and reached its maximal level at 200 mg/Kg (218.2 ± 1.5 ng/mL) compared to other infected groups. After 21 dPI, IFN-γ levels decreased in the serum of the LS-BuOH extract group at both doses towards a healthy state, and there was no significant difference between the LS-BuOH extract (200 mg/Kg) group and the healthy uninfected group. In contrast, IL-15 level was significantly ($P < 0.001$) elevated in *L. spinosa* extract groups after 10 dPI compared to infected-untreated group, reaching highest levels at the concentration of 200 mg/Kg (239.73 ± 1.1ng/mL). After 21 dPI, IL-15 levels were significantly ($P < 0.001$) lower than those of infected-untreated mice, and their levels were lowest at the concentration of 200 mg/Kg (158.67 ± 1.6 ng/mL).

Regarding TNF-α, there was a concentration-dependent decrease ($P < 0.001$) in its level in infected mice treated with *L. spinosa* extracts. *L. spinosa* butanol extract (200 mg/Kg) was

Table 1. ***C. parvum*** **oocysts' shedding in feces of infected mice groups.**

Mice Group / dPI	Untreated	NTZ treated	*L. spinosa* extracts treated						F-Value
			Ethyl acetate (LS-EtOAc)		**Ethanol** (LS-EtOH)		**Butanol** (LS-BuOH)		
			100mg/Kg	**200mg/Kg**	**100mg/Kg**	**200mg/Kg**	**100mg/Kg**	**200mg/Kg**	
Day 3	132.67 ± 1.86	131.00 ± 1.53	132.00 ± 1.15	130.30 ± 2.3	128.67 ± 4.67	131.67 ± 1.3	132.67 ± 2.85	131.00 ± 3.06	0.26^{NS}
Day 4	555.00 ± 1.53	555.67 ± 0.67	554.67 ± 2.73	554.00 ± 0.58	555.67 ± 0.88	553.33 ± 1.76	552.67 ± 1.7	554.60 ± 1.76	0.44^{NS}
Day 5	637.00 ± 5.13^{a}	542.60 ± 3.38^{e}	582.67 ± 3.18^{b}	544.67 ± 2.96^{e}	580.00 ± 1.73^{bc}	568.70 ± 2.6^{cd}	584.30 ± 7.54^{b}	558.30 ± 3.76^{d}	52.4*
Day 6	679.6. ± 2.03^{a}	582.00 ± 2^{e}	658.00 ± 1.53^{b}	609.30 ± 5.2^{d}	645.00 ± 6.66^{c}	616.00 ± 3.79^{d}	380.67 ± 3.76^{f}	328.00 ± 2.52^{g}	1206.3*
Day 7	697.00 ± 2.52^{a}	593.00 ± 3.5^{d}	670.30 ± 2.4^{b}	637.00 ± 3.61^{c}	486.00 ± 5.29^{e}	452.67 ± 5^{f}	264.67 ± 7.3^{g}	203.67 ± 4.18^{h}	1701.6*
Day 8	714.00 ± 2.3^{a}	650.30 ± 2^{d}	686.30 ± 3.76^{b}	667.00 ± 6.56^{c}	365.00 ± 5.69^{e}	307.30 ± 6.4^{f}	103.30 ± 2^{g}	74.00 ± 1.73^{h}	3889.3*
Day 9	745.30 ± 2.6^{a}	450.30 ± 3.76^{d}	702.30 ± 3.38^{b}	674.00 ± 17.5^{c}	298.67 ± 1.45^{e}	283.30 ± 2.96^{e}	93.70 ± 2.9^{f}	64.67 ± 0.88^{g}	1643.4*
Day 10	784.30 ± 5.4^{a}	426.67 ± 4.06^{d}	647.30 ± 4.6^{b}	611.00 ± 5.86^{c}	171.00 ± 1.53^{e}	120.30 ± 0.88^{f}	61.67 ± 1.2^{g}	23.70 ± 0.88^{h}	6719.6*
Day 11	705.00 ± 3.2^{a}	378.00 ± 5.29^{d}	577.30 ± 3.76^{b}	526.00 ± 2.65^{c}	164.00 ± 1.15^{e}	105.70 ± 3.18^{f}	54.67 ± 0.88^{g}	21.00 ± 1.15^{h}	7674.7*
Day 12	683.30 ± 2.4^{a}	222.00 ± 6.93^{d}	499.30 ± 2.6^{b}	444.70 ± 5.17^{c}	121.67 ± 0.88^{e}	93.30 ± 1.76^{f}	42.00 ± 1.53^{g}	12.30 ± 1.2^{h}	5144.4*
Day 13	632.30 ± 3.38^{a}	153.30 ± 7.13^{d}	295.30 ± 2.9^{b}	195.67 ± 4.37^{c}	101.00 ± 0.58^{e}	76.00 ± 4.16^{f}	24.67 ± 1.86^{g}	7.33 ± 1.2^{h}	2946.4*
Day 14	602.67 ± 3.7^{a}	95.00 ± 0.58^{d}	166.00 ± 0.58^{b}	121.70 ± 0.88^{c}	85.70 ± 1.86^{e}	57.00 ± 0.58^{f}	24.00 ± 0.58^{g}	5.00 ± 0.57^{h}	15018.8*
Day 15	528.00 ± 3.79^{a}	76.70 ± 0.88^{d}	122.30 ± 1.2^{b}	97.30 ± 0.88^{c}	70.30 ± 0.88^{e}	43.00 ± 0.57^{f}	18.67 ± 0.33^{g}	1.00 ± 0.58^{h}	12202.8*
Day 16	495.00 ± 3.2^{a}	55.00 ± 0.57^{d}	111.30 ± 0.88^{b}	84.67 ± 1.2^{c}	43.70 ± 0.33^{e}	31.00 ± 0.58^{f}	14.00 ± 0.58^{g}	0.67 ± 0.33^{h}	15217.5*
Day 17	313.67 ± 3.28^{a}	21.30 ± 1.2^{e}	96.67 ± 0.88^{b}	47.70 ± 1.45^{c}	32.67 ± 0.33^{d}	19.30 ± 0.33^{e}	8.00 ± 0.58^{f}	**0 ± 0^{g}**	5515.1*
Day 18	149.30 ± 3.48^{a}	2.00 ± 2^{e}	77.30 ± 0.88^{b}	30.70 ± 1.45^{c}	27.67 ± 0.33^{c}	11.00 ± 0.58^{d}	4.70 ± 0.33^{e}	0 ± 0^{e}	1091.8*
Day 19	55.00 ± 1.73^{a}	**0 ± 0^{e}**	25.00 ± 1.73^{b}	12.00 ± 1.15^{c}	6.00 ± 1.7^{d}	4.00 ± 1.2^{de}	1.30 ± 0.88^{e}	0 ± 0^{e}	230.8*
Day 20	0 ± 0^{c}	0 ± 0^{c}	6.00 ± 0.58^{a}	1.70 ± 0.667^{b}	2.30 ± 0.33^{b}	**0 ± 0^{c}**	**0 ± 0^{c}**	0 ± 0^{c}	40.8*
Day 21	5 ± 2.65^{a}	3.3 ± 0.88^{ab}	1.67 ± 1.2 ^{ab}	**0 ± 0^{b}**	**0 ± 0^{b}**	0 ± 0^{b}	0 ± 0^{b}	0 ± 0^{b}	3.3**

Data is expressed as Mean ± SE, Means followed by different letters indicate significance.

*Significant differences at $P < 0.001$.

**Significant differences at $P < 0.05$. dPI: days Post Inoculation, NTZ: Nitazoxanide.

https://doi.org/10.1371/journal.pone.0317497.t001

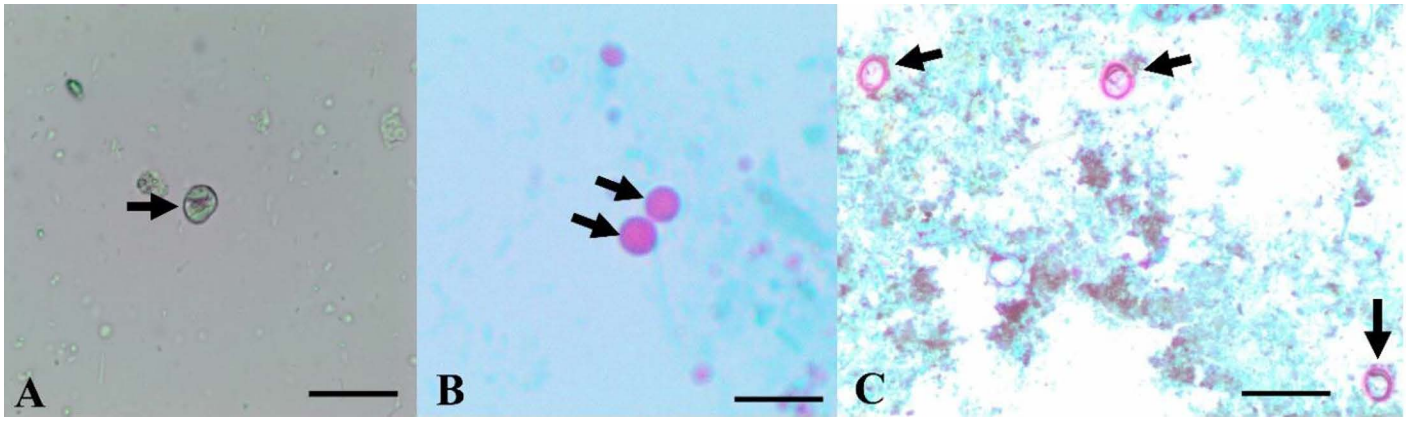

Fig 2. ***C. parvum*** **oocysts in fecal pellets of infected untreated mice.** A: Fresh fecal smear, and B: Modified Ziehl-Neelsen stained smear, 1000X). **C:** *C. parvum* oocysts in fecal pellets of infected mice which were treated with LS-BuOH extract showing oocyst shape deformation and lacking inner structures (1000X, Bar = 0.4μm).

https://doi.org/10.1371/journal.pone.0317497.g002

determined to be superior to other *L. spinosa* extracts as there was no significant differences in TNF-α levels between *L. spinosa* butanol extract (200 mg/Kg) and the healthy uninfected-untreated group (Table 3).

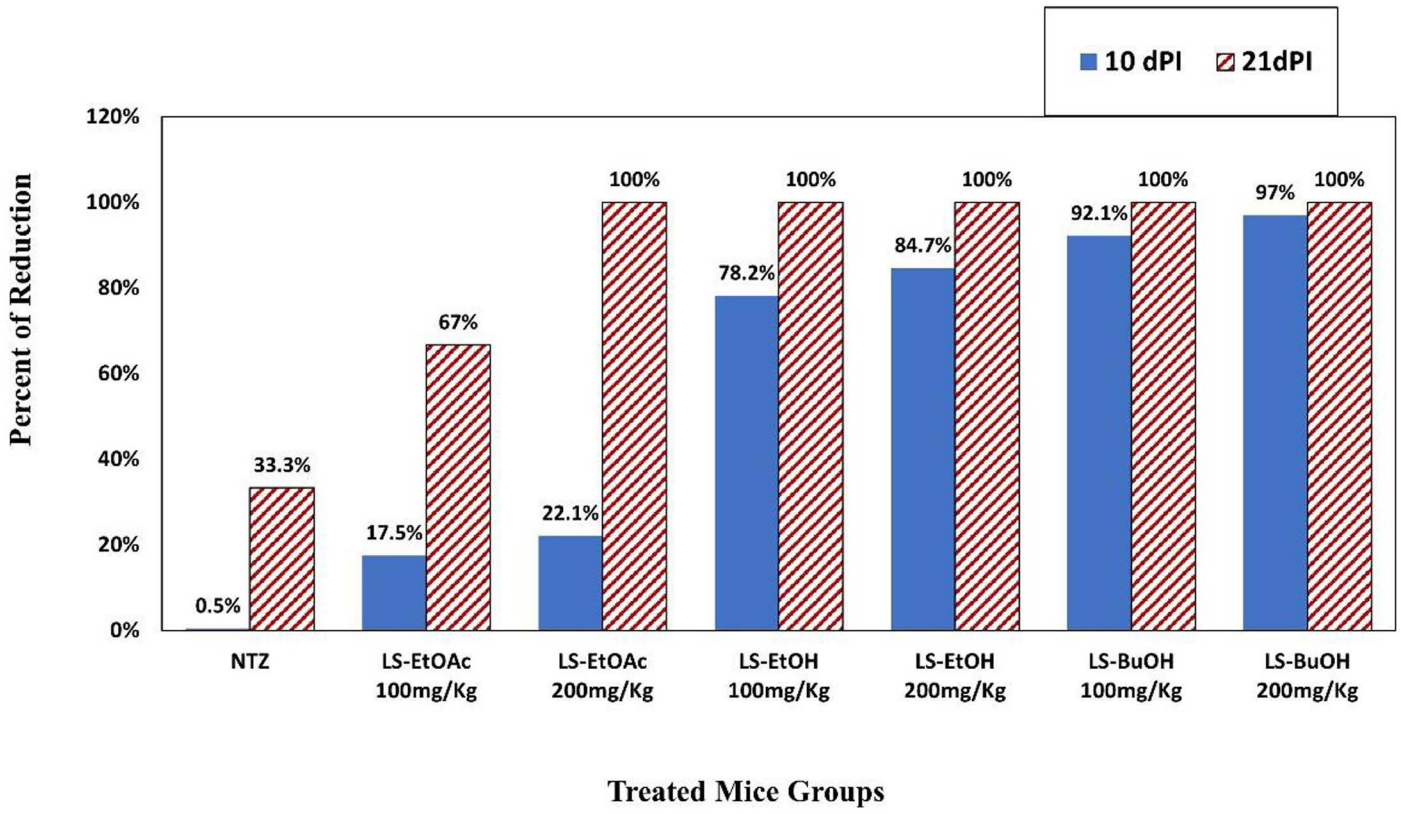

Fig 3. Percent of reduction in *C. parvum* oocysts' shedding in feces of infected and treated mice groups compared with infected non-treated mice group. dPI: days Post Inoculation, LS-EtOAc: *L. spinosa* ethyl acetate extract, LS-EtOH: *Launaea spinosa* Ethanol extract, LS-BuOH: *Launaea spinosa* Butanol extract..

https://doi.org/10.1371/journal.pone.0317497.g003

Table 2. *C. parvum* oocysts and developmental stages count in intestine of infected mice groups.

Mice Group		Untreated	NTZ treated	*L. spinosa* extracts treatment						F-Value
				Ethyl acetate (LS-EtOAc)		**Ethanol** (LS-EtOH)		**Butanol** (LS-BuOH)		
Count/dPI				**100mg/Kg**	**200mg/Kg**	**100mg/Kg**	**200mg/Kg**	**100mg/Kg**	**200mg/Kg**	
Oocysts & Developmental Stages	**10 Days**	1020 ± 5.2^{a}	833.67 ± 4.63^{b}	807.67 ± 5.93^{c}	801 ± 6.66^{c}	684.33 ± 7.54^{d}	657.67 ± 2.9^{e}	95 ± 4.51^{f}	75.67 ± 2.33^{g}	4442.59*
	21 Days	18 ± 1.53^{a}	6 ± 1.73^{b}	9 ± 1.53^{b}	4.67 ± 0.88^{bc}	1.33 ± 1^{cd}	0.33 ± 0.3^{d}	0 ± 0^{d}	0 ± 0^{d}	10.74*

Data is expressed as Mean ± SE, Means followed by different letters indicate significance.

*Significant differences at $P < 0.001$. dPI: days Post Inoculation, NTZ: Nitazoxanide.

https://doi.org/10.1371/journal.pone.0317497.t002

3.1.6. Liver functions and antioxidant assays. Concerning levels of liver enzymes, there was a significant ($P < 0.001$) elevation in ALT, AST, and ALP levels in *C. parvum* experimentally infected-untreated mice (93.26 ± 0.94, 263.5 ± 1.4, and 293.5 ± 1.4 U/L, respectively) compared to healthy uninfected-untreated ones (28.89 ± 0.82, 127.03 ± 2.3, and 203.7 ± 4.58 U/L, respectively) after 21 dPI (17 dPT). Liver enzyme levels were significantly ($P < 0.001$) lower in mice treated with Nitazoxanide or *L. spinosa* extracts compared with the infected-untreated group. Among different *L. spinosa* extracts, the greatest effect was observed in butanol extract at a dose of 200 mg/Kg as manifested by no significant differences in ALT, AST and ALP levels between this treatment and healthy group (Table 4).

As shown in Table 4, GSH–Px and catalase serum activities decreased significantly ($P < 0.001$) in *C. parvum* infected-untreated mice compared to healthy mice after 21 dPI. In

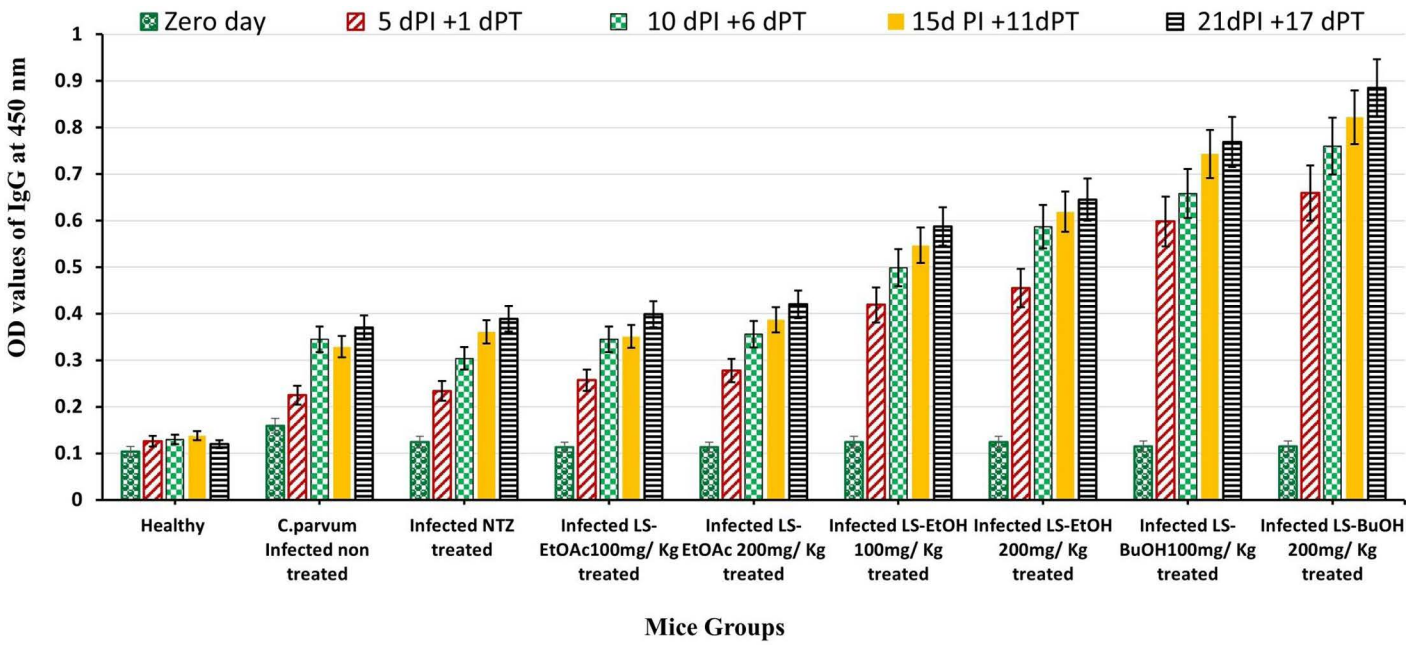

Fig 4. Serum IgG level in healthy and *C. parvum* infected mice untreated and treated groups at zero, 5, 10, 15 and 21-dPI. dPI: days Post Inoculation, dPT: days Post Treatment, *C. parvum: Cryptosporidium parvum*, LS-EtOAc: *Launaea spinosa* Ethyl acetate extract, LS-EtOH: *Launaea spinosa* Ethanol extract, LS-BuOH: *Launaea spinosa* Butanol extract.

https://doi.org/10.1371/journal.pone.0317497.g004

Table 3. Serum INF-γ, IL-15 and TNF-α levels in healthy and *C. parvum* infected mice with different treatments.

Mice Group		Uninfected untreated	Infected								F-Value
			Infected untreated	NTZ treated	*L. spinosa* extracts treatment						
					Ethyl acetate (LS-EtOAc)		**Ethanol** (LS-EtOH)		**Butanol** (LS-BuOH)		
Cytokine/dPI					100mg/Kg	200mg/Kg	100mg/Kg	200mg/Kg	100mg/Kg	200mg/Kg	
IFN-γ (ng/mL)	10 Days	78.43 ± 0.33^{h}	130.3 ± 0.58^{d}	126.7 ± 0.67^{e}	117.4 ± 0.56^{g}	$123.5 \pm 0.^{f}$	124.4 ± 0.42^{ef}	134.8 ± 0.4^{c}	195.92 ± 1.8^{b}	218.2 ± 1.5^{a}	298.16*
	21 Days	78.8 ± 0.8^{g}	165.74 ± 0.94^{a}	161.3 ± 3.02^{b}	145.09 ± 0.67^{c}	132.68 ± 0.5^{e}	139.35 ± 0.7^{d}	137.78 ± 0.74^{d}	95.09 ± 0.67^{f}	79.07 ± 0.9^{g}	521.54*
IL-15 (ng/mL)	10 Days	153.19 ± 0.9^{f}	180.6 ± 1.99^{e}	203.2 ± 1.95^{d}	206.39 ± 1^{cd}	214.6 ± 6.04^{bc}	212.3 ± 1.98^{bcd}	219.18 ± 6.9^{b}	233.3 ± 0.61^{a}	239.73 ± 1.1^{a}	2285.6*
	21 Days	151.37 ± 0.8^{h}	218.04 ± 2.25^{a}	201.37 ± 1.97^{c}	214.6 ± 0.8^{a}	206.16 ± 1.1^{b}	193.38 ± 1.2^{d}	179 ± 0.99^{e}	163.7 ± 0.79^{f}	158.67 ± 1.6^{g}	731.41*
TNF-α (ng/mL)	10 Days	84.25 ± 1.44^{f}	210.92 ± 5.07^{a}	122.17 ± 1.1^{d}	146.33 ± 1.1^{b}	141.75 ± 1.4^{bc}	136.75 ± 1.4^{c}	120.92 ± 0.8^{d}	116.75 ± 1.4^{d}	105.5 ± 0.7^{e}	63.61*
	21 Days	82.58 ± 0.83^{f}	306.75 ± 7.64^{a}	128.42 ± 2.2^{bc}	134.08 ± 1.3^{b}	121.75 ± 1.4^{cd}	124.25 ± 1.44^{c}	113.83 ± 1.1^{d}	92.58 ± 2.2^{e}	83.42 ± 2.2^{f}	332.47*

Data is expressed as Mean ± SE, Means followed by different letters indicate significance.

*Significant differences at $P < 0.001$. dPI: days Post Inoculation, NTZ: Nitazoxanide, IFN-γ: Interferon-Gamma, IL-15: Interleukin-15, TNF-α: Tumor Necrosis Factor-Alpha.

https://doi.org/10.1371/journal.pone.0317497.t003

contrast, GSH–Px and catalase were significantly ($P < 0.001$) higher in mice treated with Nitazoxanide or *L. spinosa* extracts compared to the infected-untreated group. Once again, *L. spinosa* butanol extract (200 mg/Kg) was determined to be superior to other *L. spinosa* extracts as levels were almost equal to those detected in the healthy mice group (Table 4).

3.1.7. Histopathological finding. Microscopically, normal intestinal architecture (mucosa, crypt, submucosa, muscularis layer and serosa) was detected in the healthy mice group. In contrast, the intestinal section of infected groups showed diffuse lymphoplasmacytic cells infiltrated in the lamina propria-submucosa in addition to sloughing and necrosis of lamina epithelialis, congestion of blood vessels and edema with presence of different

Table 4. Serum liver function parameters (ALT, AST and ALP) and antioxidant activity parameters (GSH-Px and Catalase) in healthy and *C. parvum* infected mice with different treatments at day 21 PI.

Mice Group / Parameter	Uninfected untreated	Infected							F-Value
		Infected untreated	NTZ treated	*L. spinosa* extracts treatments					
				Ethyl acetate (LS-EtOAc)		**Ethanol** (LS-EtOH)		**Butanol** (LS-BuOH)	
				100mg/Kg	**200mg/Kg**	**100mg/Kg**	**200mg/Kg**	**100mg/Kg**	**200mg/Kg**
ALT (U/L)	28.89 ± 0.82^{g}	93.26 ± 0.94^{a}	72.26 ± 1.39^{c}	73.95 ± 0.68^{bc}	62.7 ± 1.09^{d}	76.58 ± 1.27^{b}	58.36 ± 0.48^{e}	46.6 ± 1.05^{f}	31.26 ± 0.85^{g}	473.01*
AST (U/L)	127.03 ± 2.3^{e}	263.5 ± 1.4^{a}	193.36 ± 3^{b}	193.76 ± 2.3^{b}	183.5 ± 1.4^{c}	176 ± 2.59^{c}	161.19 ± 1.1^{d}	155.97 ± 1.6^{d}	132.37 ± 4.83^{e}	258.59*
ALP (U/L)	203.7 ± 4.58^{e}	293.5 ± 1.4^{a}	254.36 ± 1.05^{c}	268.43 ± 3^{b}	263.5 ± 1.4^{b}	262.67 ± 1.4^{b}	254.52 ± 2.2^{c}	237.97 ± 2.3^{d}	209.03 ± 3.25^{e}	127.79*
GSH-Px (U/mL)	9.09 ± 0.24^{a}	5.19 ± 0.05^{c}	6.95 ± 0.25^{b}	5.82 ± 0.35^{c}	6.98 ± 0.58^{b}	5.98 ± 0.09^{c}	6.79 ± 0.09^{b}	7.38 ± 0.12^{b}	8.98 ± 0.17^{a}	25.091*
Catalase (U/mL)	279.84 ± 0.56^{a}	210.46 ± 3.4^{e}	233.18 ± 2.6^{cd}	221.26 ± 5.5^{de}	235.3 ± 10^{cd}	233.93 ± 6^{cd}	253.19 ± 1.1^{b}	246.3 ± 2.7^{bc}	275.06 ± 2.2^{a}	23.817*

Data is expressed as Mean ± SE, Means followed by different letters indicate significance.

*Significant differences at $P < 0.001$. PI: Post Inoculation, NTZ: Nitazoxanide, ALT: Alanine aminotransferase, AST: Aspartate aminotransferase, ALP: Alkaline phosphatase, GSH-Px: Glutathione peroxidase.

https://doi.org/10.1371/journal.pone.0317497.t004

developmental stages of *C. parvum* in the intestinal epithelium and crypt of Lieberkühn that suffered from degenerative changes (Fig 5). Meanwhile, the infected-treated mice with Nitazoxanide 100 mg/Kg revealed multi-focal aggregation of inflammatory cells in lamina propria with edema. The intestine of the infected-treated mice with LS-EtOAc 100 mg/Kg exhibited sloughing and necrosis of the villous tip with congestion and edema beside the presence of *C. parvum* oocysts in intestinal crypts, causing degeneration and necrosis of intestinal crypt. On the other hand, marked edema and congestion with focal aggregation of inflammatory cells was detected in the infected-treated mice with LS-EtOAc 200 mg/Kg. Noticeable improvement was observed in the infected-treated mice with LS-EtOH 100 and 200 mg/Kg, respectively. Both groups showed mild to moderate sub-epithelial inflammatory cell infiltration, edema and sloughing of some villous lining epithelium. Marked amelioration of the intestinal histopathological alterations was detected in the infected-treated mice with LS-BuOH 200 mg/Kg within both doses as they showed the lowest lesion score compared with other treated groups. The examined intestinal sections of butanol extract likewise revealed a reduction in the injury score (Fig 5).

Regarding the histopathological lesion score, there was a statistically significant difference ($P < 0.001$) between healthy and other experimental groups except for the infected-treated mice with LS-EtOH at the dose 200 mg/Kg, and the infected-treated mice with LS-BuOH at both doses 100 mg/Kg and 200 mg/Kg. No statistically significant difference ($P > 0.05$) was detected between infected mice, the infected-treated mice with Nitazoxanide 100 mg/Kg, or the infected-treated mice with LS-EtOAc 100 mg/Kg and 200 mg/Kg. Meanwhile, the infected-treated mice with LS-EtOH 200 mg/Kg showed a significant decline ($P < 0.001$) in estimated lesion score compared to the 100 mg/Kg LS-EtOH group. Both doses of LS-BuOH (100 and 200 mg/Kg) revealed no significant difference ($P > 0.05$) as both showed the weakest intestinal lesions. Different intestinal injuries are illustrated in Fig 5.

3.1.8. Immunohistochemical assay of cleaved caspase-3 expression. Negative expression of cleaved caspase-3 was detected in the intestinal segment of the healthy untreated mice group (G1) (Fig 6A). In contrast, intense positive expression of caspase-3 was determined in the intestinal section of the *C. parvum* infected-untreated mice group (G2) (Fig 6B). Meanwhile, expression declined significantly ($P < 0.05$) in all treated groups compared to the infected group. Moderate immunoreactivity was detected in the infected-treated mice with Nitazoxanide 100 mg/Kg (Fig 6C), the infected-treated mice with LS-EtOAc 100 mg/Kg (Fig 6D), and 200 mg/Kg (Fig 6 E), respectively, though no statistically significant differences were

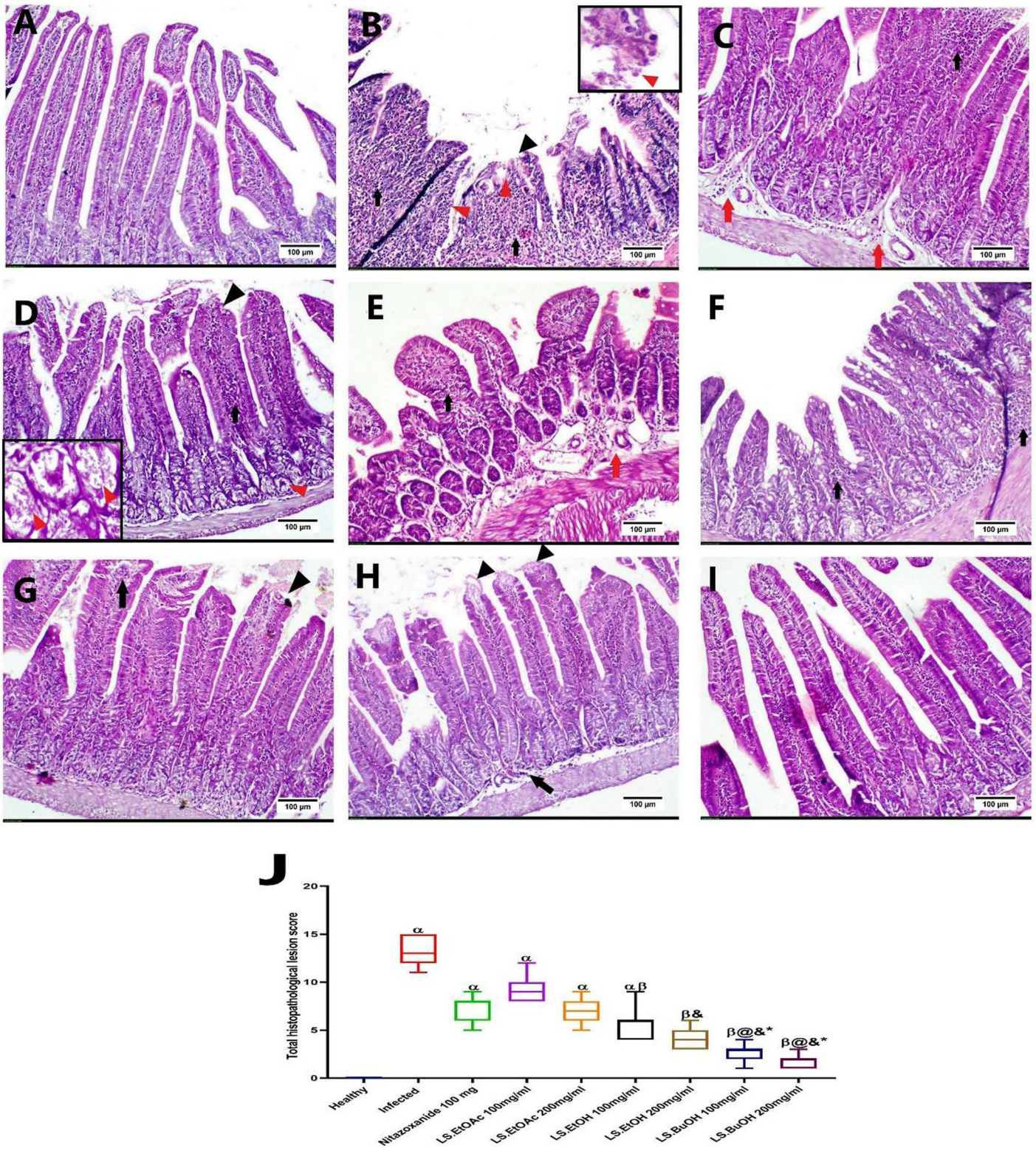

Fig 5. Representative photomicrographs showed H & E-stained intestinal sections. A) Group 1: Healthy group, showing negative expression, B) Group 2: *C. parvum* infected untreated group, C) Group 3: Infected and treated with Nitazoxanide 100mg/Kg treated group, D) Group 4: Infected and treated with *L. spinosa* ethyl acetate extract (LS-EtOAc) 100mg/Kg., E) Group 5: Infected and treated with *Ls*. EtOAc 200mg/Kg, F) Group 6: Infected and treated with *L. spinosa* ethanol extract (LS-EtOH) 100mg/Kg. G) Group 7: Infected and treated with LS-EtOH 200mg/Kg. H) Group 8: Infected and treated with *L. spinosa* butanol extract (LS-BuOH) 100mg/Kg. I) Group 9 Infected and treated with LS-BuOH 200mg. Note: inflammatory cells (black arrow), edema (red arrow), *C. parvum* oocyst (red arrowhead),

and sloughing and necrosis of villous epithelium (black arrowhead). J) Box-plot diagram representing the total histopathological lesion score among experimental groups; α: significant difference from the healthy group, β: significant difference from the infected group, @: significant difference from Nitazoxanide 100mg/Kg group, &: significant difference from *Ls.* EtOAc 100mg/Kg group, *: significant difference from *Ls.* EtOAc 200mg/Kg group. A significant difference was considered when $P < 0.05$.

https://doi.org/10.1371/journal.pone.0317497.g005

observed. Otherwise, the expression decreased significantly ($P < 0.001$) in the infected-treated mice with LS-EtOH 100 mg/Kg (Fig 6F) and LS-EtOH 200 mg/Kg (Fig 6G). Conversely, weak immunoreactivity was observed in both butanol extract groups (the infected-treated mice with LS-BuOH 100 mg/Kg (Fig 6H) and LS-BuOH 200 mg/Kg (Fig 6I)) with no statistically significant difference between them. Expression levels of cleaved caspase-3 protein are presented in Fig 6J.

3.2. UHPLC-ESI-LIT-Orbitrap-MS-based metabolites profiling of *Launaea spinosa* extracts

Reversed-phase UHPLC-ESI-LIT-Orbitrap-MS analysis was employed to holistically compare metabolite profiles of *L. spinosa* extracts *viz*. ethanol, ethyl acetate, and butanol, and to identify markers for each fraction to likely mediate for anti-parasitic effects observed in an untargeted manner. Both negative and positive ion modes were conducted to annotate 86 metabolites belonging to different classes, comprising alcohols, fatty acids, flavonoids, organic acids, phenolic acids, triterpenes, and triterpenoid saponins, as shown in Table 5. UHPLC-ESI-LIT-Orbitrap-MS negative mode chromatograms of *L. spinosa* extracts and structures of the main identified metabolic classes are shown in Fig 7 and 8, respectively. Metabolites were eluted based on their polarity, starting with the most polar compounds such as organic acids, phenolic acids, and alcohols, followed by compounds of moderate polarity, including flavonoids and triterpenoid saponins, with the least polar metabolites, fatty acids, being eluted last in the chromatogram as detailed for each metabolite class in the next subsections.

3.2.1. Identification of phenolics. Phenolic acids are commonly identified in phytochemical studies as precursors for numerous phenolic metabolites. They are detected either as free or conjugated with sugars and various organic acids [38]. Owing to their significant polarity, phenolic acids typically appear earlier in chromatographic analyses, primarily under negative ion mode, which aligns with their acidic nature. Twenty-three phenolic acids were identified in *L. spinosa* extracts, 16 of which (**7**, **10**, **17**–**21**, **24**–**27**, **31**, **37**, **40**, **42 & 45**) belonged to hydroxycinnamic acid derivatives, whereas the remaining 7 peaks (**5**, **8**, **9**, **11**, **12**, **30** & **32**) belonged to hydroxybenzoates, Table 5. The identified cinnamates were detected as either free or conjugated with sugars or organic acids. Caffeoylquinic acid conjugates were the main identified ones with mono-, di-, or tri-*O*- caffeoyl moieties. Peaks **10**, **17**, **18**, and **21** at *m/z* 353.0876 $C_{16}H_{17}O_9^-$ exhibited UV spectra typical of caffeoylquinic acid, alongside two characteristic fragments at *m/z* 179 and 191 for caffeic and quinic acids, respectively, and were annotated as positional isomers of caffeoyl quinic acid, as shown in **Fig.** S1 in S1 File. Similarly, peaks **26**, **37**, and **42** showed similar mass spectra at *m/z* 515.1193 $C_{25}H_{23}O_{12}^-$ with extra loss of 162 amu equivalent to a caffeoyl moiety and were annotated as di-*O*-caffeoylquinic acid positional isomers as shown in **Fig.** S2 in S1 File. Likewise, peak **45** at *m/z* 677.1506 $C_{34}H_{29}O_{15}^-$ showed characteristic fragments at 515 and 353 amu due to successive loss of caffeoyl moieties, and were annotated as tri-*O*-caffeoylquinic acid as shown in Table 5 [39].

Compared to cinnamate derivatives, derivatives of hydroxybenzoic acid displayed a distinctive fragment at *m/z* 153 and 135 corresponding to dihydroxy and hydroxybenzoic acids, respectively [38]. Peaks **8** and **12** $[M\text{-}H]^-$ at *m/z* 153.0196 $C_7H_5O_4^-$ were annotated

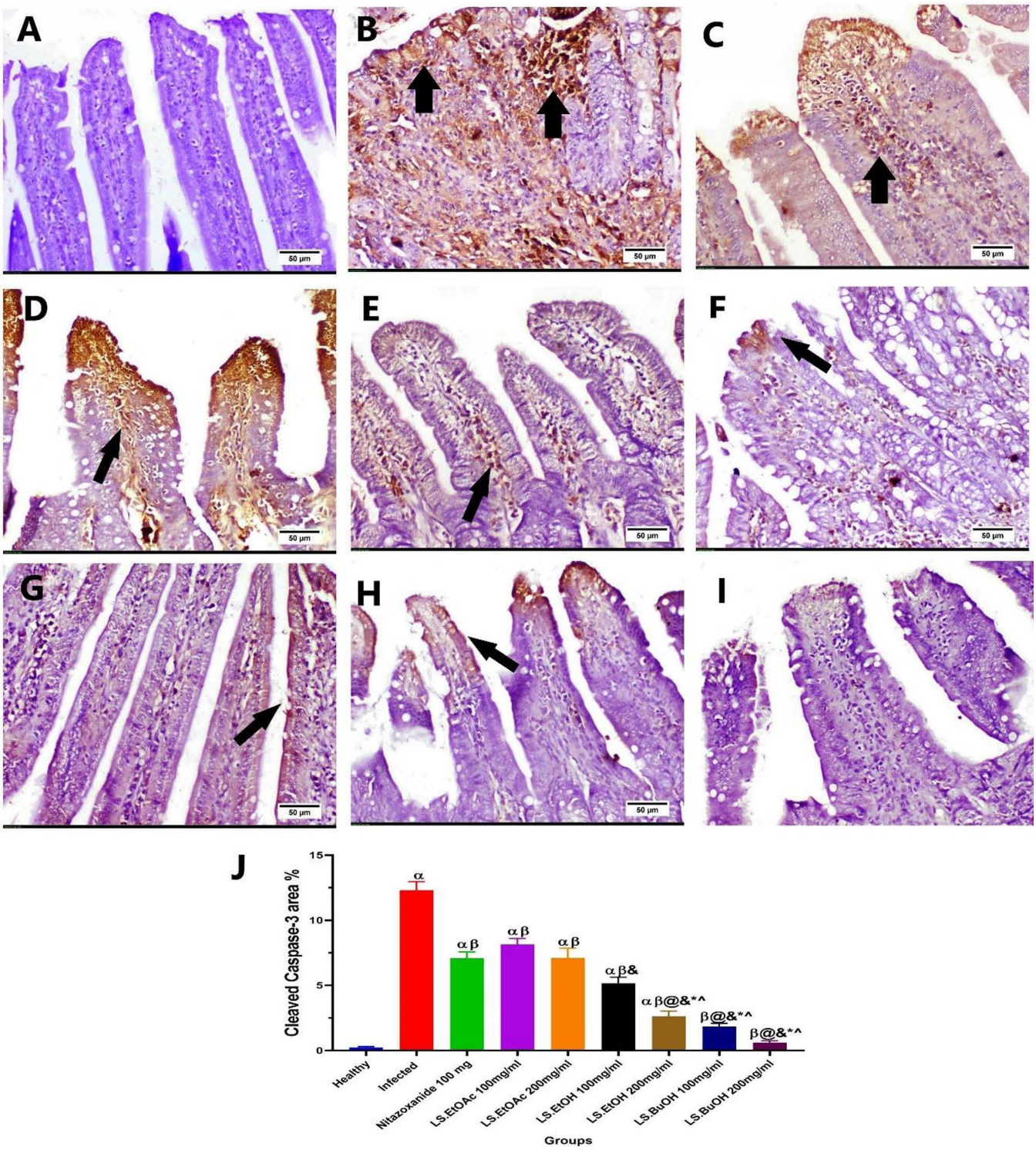

Fig 6. Representative photomicrographs of cleaved Caspase-3 immune-stained intestinal section. A) Group 1: Healthy group, showing negative expression, B) Group 2: *C. parvum* infected untreated group, C) Group 3: Infected and treated with Nitazoxanide 100mg/Kg treated group, D) Group 4: Infected and treated with *L. spinosa* ethyl acetate extract (LS-EtOAc) 100mg/Kg., E) Group 5: Infected and treated with *Ls.* EtOAc 200mg/Kg, F) Group 6: Infected and treated with *L. spinosa* ethanol extract (LS-EtOH) 100mg/Kg. G) Group 7: Infected and treated with LS-EtOH 200mg/Kg. H) Group 8: Infected and treated with *L. spinosa* butanol extract (LS-BuOH) 100mg/Kg. I) Group 9 Infected and treated with LS-BuOH 200mg/. Note: black arrow indicates positive expression. J) Chart representing the cleaved Caspase-3 area percent among experimental groups; α: significant difference from the healthy group,

β: significant difference from the infected group, @: significant difference from Nitazoxanide 100mg/Kg group, &: significant difference from LS-EtOAc 100mg/Kg, *: significant difference from LS-EtOAc 200mg/Kg, ^ significant difference from LS-EtOH 100mg/Kg. Data presented as mean ± standard deviation (SD). A Significant difference was considered when $P < 0.05$.

https://doi.org/10.1371/journal.pone.0317497.g006

Table 5. Metabolites identified in the different *L. spinosa* extracts using UHPLC-ESI-MS in negative/ positive ionization modes.

No.	Rt (min)	UV	Metabolite	$[M-H]^-$/ $[M+H]^+$ (m/z)	Error (ppm)	Elemental composition	MS^n product ions	*L. spinosa* extract		
								EtOAc	EtOH	BuOH
1	0.51	191, 295	Quinic acid	191.0565	1.8	$C_7H_{11}O_6^-$		+	+	+
2	0.58	n.d.	Malic acid	133.0147	2.5	$C_4H_5O_5^-$	115, 87, 71	+	+	+
3	0.63	n.d.	Citric acid	191.0200	3.5	$C_6H_7O_7^-$	173, 111	+	+	+
4	0.70	n.d.	Succinic acid	117.0197	2.5	$C_4H_5O_4^-$	99, 73	+	+	+
5	1.10	264, 321	Protocatechuic acid-*O*-hexoside	315.0721	0.0	$C_{13}H_{15}O_9^-$		+	+	+
6	1.18	264, 310	Piscidic acid	255.0512	0.8	$C_{11}H_{11}O_7^-$	237, 211, 193, 179, 165, 149	+	+	+
7	1.29	277, 310	Ferulic acid	193.0509	1.5	$C_{10}H_9O_4^-$		+	+	+
8	1.60	259, 289	Dihydroxybenzoic acid	153.0196	1.3	$C_7H_5O_4^-$	135, 123, 109, 91	+	+	–
9	1.87	268	Syringic acid-*O*-hexosie	359.0983	−0.1	$C_{15}H_{19}O_{10}^-$	197, 153	+	+	+
10	2.05	277, 327	*O*-Caffeoylquinic acid	353.0876	−0.6	$C_{16}H_{17}O_9^-$	191, 179, 173, 161, 135	+	+	+
11	2.54	236, 295	Hydroxybenzoic acid	137.0248	2.6	$C_7H_5O_3^-$	119, 110, 93, 66	+	+	+
12	2.68	259, 289	Dihydroxybenzoic acid isomer	153.0196	1.3	$C_7H_5O_4^-$	135, 123, 109, 91	+	–	–
13	2.82	n.d.	Hydroxyheptanedioic acid	175.0615	1.5	$C_7H_{12}O_5^-$	157, 147, 131, 115, 113, 85	+	–	–
14	3.17	259	Coniferyl alcohol sulfate	259.0282	0.6	$C_{10}H_{11}O_6S^-$	229, 179, 161	+	+	+
15	3.72	259	Coniferyl alcohol sulfate Isomer	259.0283	0.5	$C_{10}H_{11}O_6S^-$	229, 179, 161	+	+	+
16	4.02	289	Eucomic acid	239.0562	0.5	$C_{11}H_{11}O_6^-$	221, 177, 163, 149, 133, 91	+	+	+
17	4.17	304, 327	*O*-Caffeoylquinic acid isomer1	353.0877	−0.4	$C_{16}H_{17}O_9^-$	191, 179, 173, 161, 135	+	+	+
18	4.64	299, 325	*O*-Caffeoylquinic acid isomer2	353.0876	−0.6	$C_{16}H_{17}O_9^-$	191, 179, 173, 161, 135	+	+	+
19	4.95	251, 327	Caffeic acid	179.0351	0.7	$C_9H_7O_4^-$	161, 151, 135, 107	+	–	$^+$
20	4.97	260, 316	Ferulic acid sulfate	273.0074	−0.1	$C_{10}H_9O_7S^-$	229, 193, 149, 79	+	+	+
21	5.95	290, 326	*O*-Caffeoylquinic acid isomer3	353.0876	−0.7	$C_{16}H_{17}O_9^-$	191, 179, 173, 161, 137, 135, 111	+	+	+
22	7.36	n.d.	Dihydroxy-(methylpropyl) butanedioic acid-*O*-rhamnoside	351.1297	0.0	$C_{14}H_{23}O_{10}^-$	333, 315, 291, 267, 249, 231, 205, 175, 157, 113	+	+	+
23	8.45	293, 325	Methyl jasmonate-*O*-hexoside	431.1920	−0.6	$C_{20}H_{31}O_{10}^-$	385, 223, 205, 179, 153	+	+	+
24	8.57	291, 323	Hydroxyferuloyl-*O*-hexoside	371.0982	-0.4	$C_{16}H_{19}O_{10}^-$	353, 249, 231, 209, 193, 175, 157, 121	+	+	+
25	8.71	297, 313	Sinapoyl-hexoside	385.1170	7.8	$C_{17}H_{21}O_{10}^-$	325, 263, 241, 223, 181, 151, 121	+	–	$^+$
26	8.81	294, 327	Di-*O*-caffeoylquinic acid	515.1193	−0.5	$C_{25}H_{23}O_{12}^-$	353, 191, 179, 173	+	+	+
27	8.97	295, 321	Caffeoylquinic acid methyl ether	367.1032	2.2	$C_{17}H_{19}O_9^-$	191, 173	+	+	+
28	9.11	219, 334	Coniferin sulfate	421.0810	8.0	$C_{16}H_{21}O_{11}S^-$	241, 179	+	+	+
29	9.16	n.d.	Octanedioic acid	173.0822	1.3	$C_8H_{13}O_4^-$	111	+	+	–
30	9.48	261, 309	Hydroxybenzoic acid isomer	137.0247	2.1	$C_7H_5O_3^-$	93	+	+	–
31	9.55	295, 330	Caftaric acid-*O*-hexoside	473.0723	−0.6	$C_{22}H_{17}O_{12}^-$	311, 293	+	–	–
32	9.56	335	*O*-Galloyl-*O*-(4-hydroxybenzoyl)-hexoside	451.0915	7.2	$C_{20}H_{19}O_{12}^-$	435, 371, 311, 257, 241, 177	–	–	$^+$
33	9.73	288, 369	Quercetin-*O*-rhamnosyl-hexoside	609.1458	−0.5	$C_{27}H_{29}O_{16}^-$	463, 447, 301, 271, 255	+	+	+
34	9.76	288, 369	Quercetin-*O*-hexoside	463.0881	−0.3	$C_{21}H_{19}O_{12}^-$	301	+	–	$^+$
35	10.03	270, 330	Luteolin-*O*-rhamnosyl-hexoside	593.1509	−0.4	$C_{27}H_{29}O_{15}^-$	447, 285, 257, 213, 185, 171	+	+	+
36	10.10	294, 335	Tetrahydroxymethoxyflavone-*O*-rhamnosyl-hexoside	623.1617	-0.1	$C_{28}H_{21}O_{16}^-$	477, 447, 315, 299, 271, 255	+	+	+

(Continued)

Table 5. (Continued)

No.	Rt (min)	UV	Metabolite	$[M-H]^-$/ $[M+H]^+$ (m/z)	Error (ppm)	Elemental composition	MS^n product ions	*L. spinosa* extract		
								EtOAc	EtOH	BuOH
37	10.12	295, 325	Di-*O*-caffeoylquinic acid isomer 1	515.1194	−0.2	$C_{25}H_{23}O_{12}^-$	353, 335, 191, 179	+	+	+
38	10.27	n.d.	Nonanedioic acid (Azelaic acid)	187.0978	1.4	$C_9H_{15}O_4^-$	169, 125, 97	+	+	–
39	10.53	286, 321	Tetrahydroxyflavane-*O*-hexoside	435.0966	7.5	$C_{20}H_{19}O_{11}^-$	343, 311, 249, 273, 241, 151	+	+	+
40	10.62	290, 323	*O*-Caffeoylferuloylquinic acid	529.1350	0.2	$C_{26}H_{25}O_{12}^-$	367, 353, 349, 335, 191, 179, 161	+	+	–
41	10.68	296, 324	Acacetin	285.0764	2.4	$C_{16}H_{13}O_5^+$		+	–	–
42	10.72	297, 325	Di-*O*-caffeoylquinic acid isomer 2	515.0497	5.8	$C_{25}H_{23}O_{12}^-$	497, 435, 395, 377, 353, 335, 255, 191, 179	+	+	+
43	10.93	n.d.	Dihydroxy-oxo-oleanenoic acid-*O*-dihexoside sulfate	889.3892	3.2	$C_{42}H_{65}O_{18}S^-$	845, 727, 683, 647, 603, 441, 401, 255	+	+	+
44	11.06	n.d.	Dihydroxy-oleanenoic acid-*O*-dihexoside	809.4326	−0.7	$C_{42}H_{65}O_{15}^-$	765, 647, 603, 585, 455, 391	+	+	+
45	11.10	289, 321	Tri-*O*-caffeoylquinic acid	677.1506	−0.8	$C_{34}H_{29}O_{15}^-$	515, 497, 353, 335	+	+	+
46	11.14	n.d.	Dihydroxy-oxo-oleanenoic acid-*O*-dihexoside sulfate isomer	889.3892	3.2	$C_{42}H_{65}O_{18}S^-$	845, 727, 683, 603, 441, 401, 255	–	+	+
47	11.18	n.d.	Dihydroxy-oleanenoic acid-*O*-dihexosyl-pentoside sulfate	1007.4519	−0.8	$C_{47}H_{75}O_{21}S^-$	977, 845, 683, 653, 603, 471	–	+	+
48	11.18	n.d.	Dihydroxy-oxo-oleanenoic acid-*O*-dihexosyl-rhamnoside	955.4912	0.4	$C_{48}H_{75}O_{19}^-$	833, 793, 749, 731, 705, 629, 587, 569, 455, 441	+	–	–
49	11.22	n.d.	Unknown triterpenoid saponin	859.3789	0.1	$C_{41}H_{63}O_{17}S^-$	815, 697, 653, 573, 483, 441	+	+	+
50	11.44	n.d.	Dihydroxy-oxo-oleanenoic acid-*O*-hexoside	931.3999	3.8	$C_{47}H_{63}O_{19}^-$	887, 769, 725, 683, 441, 423, 283	+	+	+
51	11.51	n.d.	Dihydroxy-oxo-oleanenoic acid-*O*-hexosyl-rhamnoside sulfate	873.3945	0.2	$C_{42}H_{65}O_{17}S^-$	829, 711, 667, 649, 587, 441, 401, 297	+	+	+
52	11.57	n.d.	Oleanene-diol-*O*-malonyl-dihexoside	851.4434	0.0	$C_{44}H_{67}O_{16}^-$	833, 807, 747, 689, 645, 603, 483, 441	+	–	–
53	11.69	n.d.	Unknown triterpenoid saponin	845.3993	4.1	$C_{44}H_{61}O_{16}^-$	815, 683, 653, 471, 441	+	+	+
54	11.86	n.d.	Tetrahydroxy-octadecenoic acid	345.2284	0.5	$C_{18}H_{33}O_6^-$	327, 309, 291	+	+	–
55	11.90	n.d.	Dihydroxy-oxo-oleanenoic acid-*O*-hexoside	647.3803	0.3	$C_{36}H_{45}O_{10}^-$	603, 565, 525, 513, 483, 455, 441	+	+	–
56	11.98	n.d.	Hydroxy-oleanenoic acid-*O*-dihexosyl-hexouronide	955.4906	−0.2	$C_{48}H_{75}O_{19}^-$	793, 631, 455, 437	+	+	+
57	11.99	n.d.	Dihydroxy-oxo-oleanenoic acid-*O*-hexoside sulfate	727.3370	0.4	$C_{36}H_{55}O_{13}S^-$	683, 603, 563, 485, 441, 423, 259	+	+	–
58	12.01	n.d.	Trihydroxy-octadecenoic acid	329.2334	3.6	$C_{18}H_{33}O_5^-$	293, 229, 211, 171	+	+	–
59	12.03	n.d.	Unknown triterpenoid saponin	1019.4526	−2.6	$C_{48}H_{75}O_{21}S^-$	857, 737, 607, 575, 510, 401, 357, 321	+	+	+
60	12.15	n.d.	Dihydroxy-oxo-oleanenoic acid-*O*-hexoside sulfate	727.3367	−0.2	$C_{36}H_{55}O_{13}S^-$	683, 667, 637, 603, 593, 596, 483, 441, 423, 370	+	+	–
61	12.26	n.d.	Oleanene-diol-*O*-hexoside	603.3904	0.2	$C_{35}H_{55}O_8^-$	441, 423, 391, 347, 327	+	+	–
62	12.36	n.d.	Hydroxy-oleanenoic acid-*O*-hexosyl-hexouronide	793.4374	-0.8	$C_{42}H_{65}O_{14}^-$	631, 613, 569, 455	+	+	+
63	12.42	n.d.	Hydroxy-oleanenoic acid-*O*-hexoside sulfate	697.3261	4.5	$C_{35}H_{54}O_{12}S^-$	653, 635, 617, 573, 485, 455, 441, 411	+	+	+
64	12.48	n.d.	Unkown triterpenoid saponin	1019.4517	−1.0	$C_{48}H_{75}O_{21}S^-$	939, 857, 401, 357, 321	–	–	+
65	12.52	n.d.	Trihydroxy-octadecadienoic acid	327.2180	0.9	$C_{18}H_{31}O_5^-$	309, 291, 247	+	+	+
66	12.80	n.d.	Dihydroxy-oleanenoic acid-*O*-pentoside-sulfate	683.3467	5.3	$C_{35}H_{55}O_{11}S^-$	639, 603, 638, 471, 210	+	+	+

(Continued)

Table 5. (Continued)

No.	Rt (min)	UV	Metabolite	[M-H]⁻/ [M+H]⁺ (m/z)	Error (ppm)	Elemental composition	MSⁿ product ions	*L. spinosa* extract		
								EtOAc	EtOH	BuOH
67	12.84	n.d.	Trihydroxy octadecatrienoic acid	325.2022	2.2	$C_{18}H_{29}O_5^-$	307, 289, 281, 271, 263, 151, 137, 125	–	+	+
68	12.87	n.d.	Hydroxy-oleanenoic acid-*O*-hexosyl-pentoside-sulfate	829.4045	-0.5	$C_{41}H_{65}O_{15}S^-$	667, 587, 455, 373	+	+	+
69	13.22	n.d.	Hydroxy-oleanenoic acid-*O*-hexosyl-hexouronide isomer	793.4374	-0.7	$C_{42}H_{65}O_{14}^-$	749, 731, 631, 613, 587, 569, 537, 523, 513, 455, 437	+	+	+
70	13.45	n.d.	Dihydroxy-oleanenone	441.3371	0.0	$C_{29}H_{45}O_3^-$	399, 373, 361, 343, 325, 307	+	+	+
71	13.51	n.d.	Unknown triterpenoid saponin	1075.5139	1.8	$C_{55}H_{79}O_{21}^-$	1045, 913, 883, 767, 669, 627, 455, 401	–	–	+
72	13.79	n.d.	Dihydroxy-octadecenoic acid	313.2384	-0.1	$C_{18}H_{33}O_4^-$	295, 277, 201, 171	+	+	+
73	14.17	n.d.	Dihydroxy-hexadecenoic acid	285.2074	1.0	$C_{16}H_{29}O_4^-$	267, 223	+	+	+
74	14.58	n.d.	Dihydroxy-octadecadienoic acid	311.2230	0.6	$C_{18}H_{31}O_4^-$	293, 249	+	+	+
75	15.09	n.d.	Dihydroxy-octadecenoic acid	313.2387	0.1	$C_{18}H_{33}O_4^-$	295, 251	+	+	+
76	15.41	n.d.	Unknown diterpene	339.2542	3.4	$C_{20}H_{35}O_4^-$	321, 295, 277, 253, 183	+	+	+
77	15.49	n.d.	Glycerol-dihydroxyeicosenoate	415.3065	-0.1	$C_{23}H_{43}O_6^-$	397, 377, 341, 323, 279, 241, 191	+	+	+
78	15.58	n.d.	Dihydroxy-nonadecenoic acid	327.2544	4.2	$C_{19}H_{35}O_4^-$	309, 255	+	+	–
79	15.84	n.d.	Hydroxyoctadecadienoic acid	295.2281	4.5	$C_{18}H_{31}O_3^-$	277, 249, 231, 193, 155, 141	+	+	–
80	15.97	n.d.	Dihydroxy-eicosenoic acid	341.2697	-0.2	$C_{20}H_{37}O_4^-$	323, 279	+	+	+
81	16.15	n.d.	Unknown triterpene	517.2805	-0.3	$C_{29}H_{41}O_8^-$	473, 441, 297, 219, 175	+	+	+
82	16.24	n.d.	Hydroxyhexadecanoic acid	271.2281	0.7	$C_{16}H_{31}O_3^-$	253, 225, 209	+	+	–
83	16.36	n.d.	Acetylglycerol-dihydroxyeicosenoate	457.3171	2.4	$C_{25}H_{45}O_7^-$	441, 415, 397, 395, 369, 341, 323, 279	+	+	–
84	16.91	n.d.	Eicosanedioic acid	369.3010	-0.1	$C_{22}H_{41}O_4^-$	351, 307	+	+	+
85	17.40	n.d.	Hydroxydocosanoic acid	355.3216	-0.4	$C_{22}H_{43}O_3^-$	337, 309, 295	+	+	–
86	17.89	n.d.	Dihydroxytetracosenoic acid	397.3323	2.8	$C_{24}H_{45}O_4^-$	379, 353, 335	+	–	–

(+) and (-) indicate presence and absence of a metabolite, respectively; n.d., not detected; EtOH, ethanol extract; EtOAc, ethyl acetate extract; BuOH, butanol extract.

https://doi.org/10.1371/journal.pone.0317497.t005

as dihydroxybenzoic acid positional isomers. Their mass spectrum showed characteristic fragments at *m/z* 135, 109, and 91 due to loss of $[M\text{-}H_2O]^-$, $[M\text{-}CO_2]^-$, and $[M\text{-}CO_2\text{-}H_2O]^-$, respectively (**Fig.** S3 in **S1 File**). It should be noted that hydroxybenzoates were detected at trace levels in comparison to hydroxycinnamates, inferring that *L. spinosa* biosynthesis is activated towards cinnamates production, and in accordance with that previously identified in *L. mucronata*. [13]

This study represents the first *L. spinosa* phenolic acids profile, noting that their levels were higher in butanol extract than other extracts, which likely accounted for its significant biological activity compared to other extracts.

3.2.2. Identification of organic acids. Eleven organic acids (**1**–**4**, **6**, **13**, **16**, **22**–**23**, **29** & **38**) were detected early in the chromatogram owing to their high polarity. Their annotation was based on MS^2 fragments of -18 and -44 amu due to the loss of H_2O molecules and carboxyl group, respectively [40]. For example, peak **2** at *m/z* 133.0170 $C_4H_5O_5^-$ showed such a fragmentation pattern and was annotated as malic acid (**Fig.** S4 in **S1 File**). The identified organic acids were previously detected in *Launaea mucronate* ethanolic extract [13], while this is the first report of an organic acids profile in *L. spinosa*.

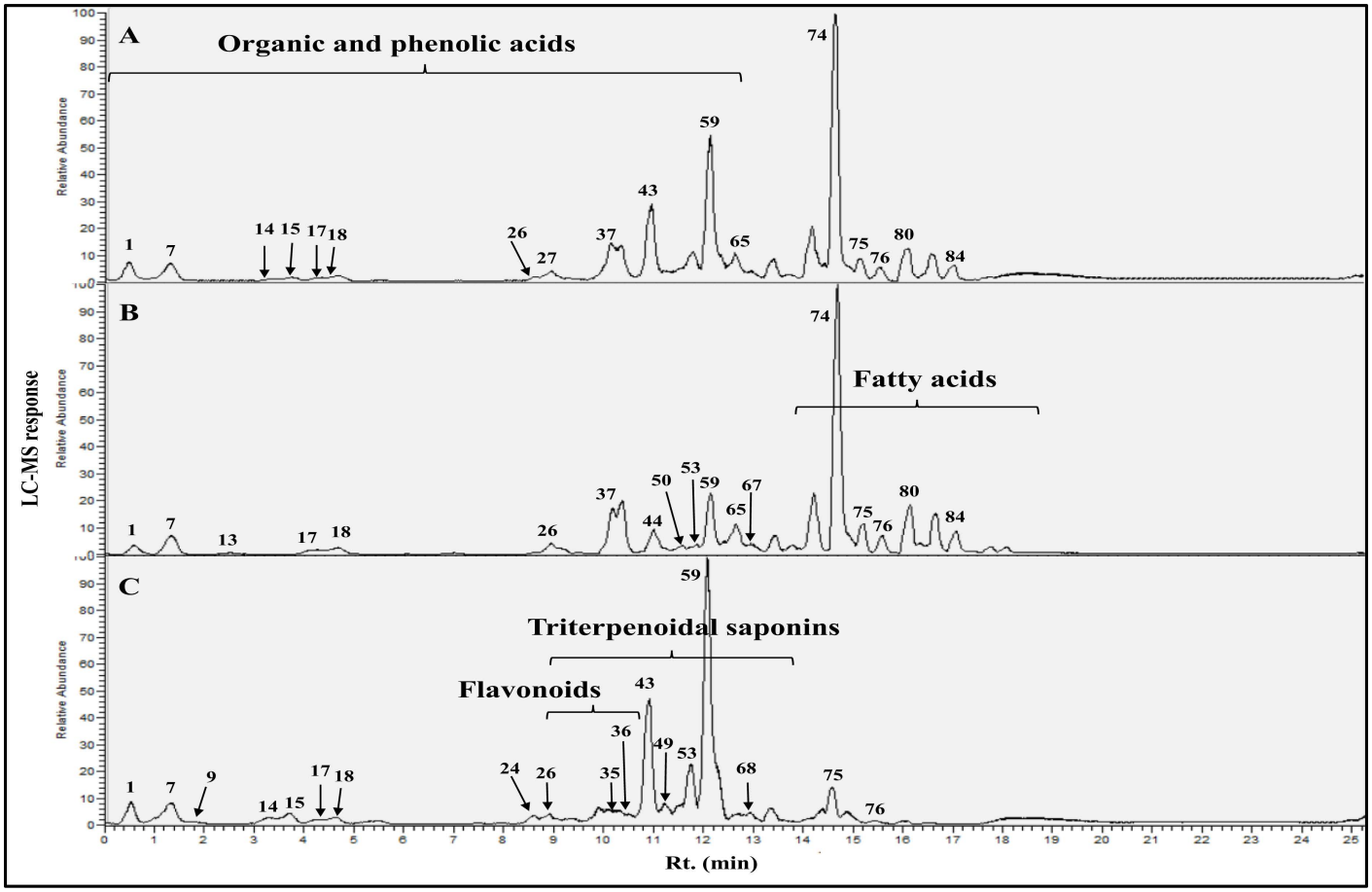

Fig 7. Representative UPLC-ESI-MS negative ionization mode spectra of the different *L. spinosa* extracts. (**A**) ethyl acetate, (**B**) ethanol, and (**C**) butanol. Assigned peak numbers follow that shown in Table 5.

https://doi.org/10.1371/journal.pone.0317497.g007

3.2.3. Identification of flavonoids. Six chromatographic peaks (**33–36**, **39** & **41**) were identified as flavonoids and their conjugates based on their UV spectra (200–600 nm). The identified flavonoids belonged to flavones (**35**, **36** & **41**), flavonol (**33 & 34**), and flavane (**39**) as shown in Table 5. Flavones exhibited UV max at 270 nm (Band II) and 335–350 nm (Band I). For example, peak **35** at *m/z* 593.1509 $C_{27}H_{29}O_{15}^-$ showed two characteristic losses of -146 and -162 amu equivalent to rhamnosyl and hexosyl moieties, respectively, and were annotated as luteolin-*O*-rhamnosyl-hexoside as shown in **Fig.** S5 in **S1 File**. [41].

Flavonols exhibited UV max at 250–275 nm (Band II) and 352–380 nm (Band I). For example, peak **33** at *m/z* 609.14581 $C_{27}H_{29}O_{16}^-$ showed similar -146 and -162 amu losses yielding quercetin aglycone and were annotated as quercetin-*O*-rhamnosyl-hexoside as shown in **Fig.** S6 in **S1 File** [42].

It is important to highlight that flavonoids were identified at trace levels, which suggests that major secondary metabolites in *L. spinosa* included triterpenoid saponins and phenolic acids as shown in Table 5. Flavonoid concentration was significantly higher in butanol extract in comparison to ethyl acetate and ethanol owing to their increased polarity.

3.2.4. Identification of triterpenoid saponins. Twenty-one triterpenoid saponins of oleanane skeleton were detected in different extracts of *L. spinosa*, particularly in the butanol extract owing to their improved recovery in that solvent (Table 5) and suggestive that butanol

is the richest in that class. The major identified saponins aglycones were hydroxy-oleanenoic acid (*m/z* 455) in peaks **56**, **62**, **63**, **68**, and **69**, dihydroxy-oleanenoic acid (*m/z* 472) in peaks **44**, **47**, and **61**, dihydroxy-oxo-oleanenoic acid (*m/z* 486) in peaks **43**, **46**, **48**, **50**, **51**, **53**, **55**, **57**, and **60**, and **66**, oleanene-diol (*m/z* 442) [38]. The triterpenoidal type saponins were assigned based on the loss of -44 amu for carboxylic acid group, with detection predominantly occurring in negative ionization mode. The identification of glycosides type was determined from the neutral losses of -86, -132, -146, -162, and -176 corresponding to malonyl, pentose, deoxyhexose, hexose, and hexuronic acid, respectively [43]. For example, peak **56** at *m/z* 955.4906 $C_{48}H_{75}O_{19}^-$ showed three successive losses of -162, -162, and -176 amu equivalent to two hexosyl units and hexuronic acid, respectively. This fragmentation yielded a triterpenoid aglycone at *m/z* 455 equivalent to hydroxy-oleanenoic acid, assigned as hydroxy-oleanenoic acid-*O*-dihexosyl-hexouronide (**Fig**. S7 in **S1 File**).

Nine sulfated triterpenoidal saponins (**43**, **46**, **47**, **51**, **57**, **60**, **63**, **66**, and **68**) were detected for the first time in *L. spinosa*. Sulfate esters were identified in negative mode by their distinctive neutral loss of -80 amu [44]. For instance, peaks **47** and **68** at *m/z* 1007.4519 $C_{47}H_{75}O_{21}S^-$ and *m/z* 829.4045 $C_{41}H_{65}O_{15}S^-$ exhibited the fragmentation pattern of triterpenoidal saponins. Additionally, a characteristic loss of sulfate ester was detected, assigned as dihydroxy-oleanenoic acid-*O*-di-hexosyl-pentoside sulfate and hydroxy-oleanenoic acid-*O*-hexosyl-pentoside-sulfate (**Fig.** S8 in **S1 File** and S9 in **S1 File**, respectively). Despite the ability to identify many triterpenoidal saponins, it was impossible to provide a clear structure assignment due to the inability to determine the precise location of functional groups.

It's noteworthy that triterpenoid saponins exhibited the highest relative levels in the butanol extract, which likely accounts for its superior biological action in comparison to other extracts, *i.e.*, ethyl acetate and ethanol. This is the first report of the presence of sulfated triterpenoid saponins in genus *Launaea* and should be pursued in other species for conclusive note of its distribution pattern.

3.2.5. Identification of fatty acids. In the later elution region of the chromatogram, 15 fatty acid peaks were eluted due to their nonpolar nature, and for the same reason, their amounts were higher in ethyl acetate extract (**Table 5**). These fatty acids belonged to unsaturated, mono-, and polyunsaturated fatty acids. The identified unsaturated fatty acids were oxygenated, *i.e.*, hydroxy (**79**), dihydroxy (**72–75**, **78**, **79**, and **86**), trihydroxy (**58**, **65**, and **67**), or tetrahydroxy (**54**) fatty acids as shown in **Table 5**. Hydroxy fatty acids were annotated based on the loss of extra water molecule(s) in negative ionization mode. For example, peak **67** annotated as trihydroxy octadecatrienoic acid showed a molecular mass at *m/z* 325.2022 $C_{18}H_{29}O_5^-$ and three characteristic fragment ions at *m/z* 307, 289, and 271 due to three successive losses of H_2O, alongside another key fragment at *m/z* 281 due to the loss of CO_2 (**Fig.** S10 in **S1 File**). Hydroxy fatty acids have previously been attributed for anti-inflammatory and anticancer effects [45]. Compared to an abundance of unsaturated fatty acids, only three saturated fatty acids, *i.e.*, peaks **82**, **84**, and **85,** were detected as hydroxyhexadecanoic acid, eicosanedioic acid, and hydroxydocosanoic acid, respectively (**Table 5**).

3.3. Correlation between bioactivities and major metabolites in *L. spinosa* extracts

Supervised partial least square (PLS) was utilized to assess the relationship between identified metabolites *via* UPLC-MS (X-variables) and the anti-parasitic activities conducted in the present study. Partial Least Square biplot (**Fig. 9A**), represented by score and loading plots, revealed a clear distinction between the three different *L. spinosa* extracts and variables contributing to their separations (R2X = 86%). Interestingly, the biological activity parameters

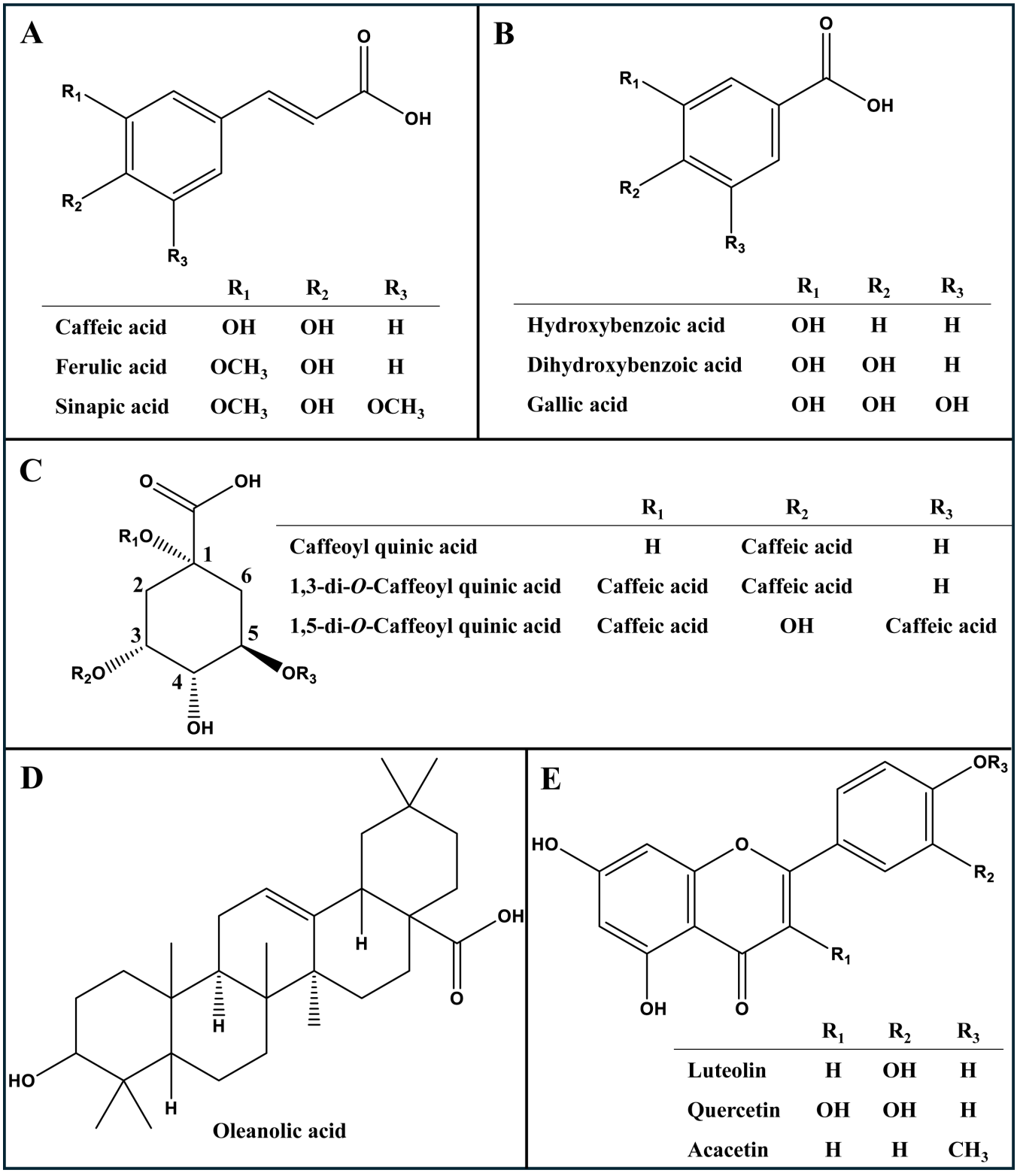

	R_1	R_2	R_3
Caffeic acid	OH	OH	H
Ferulic acid	OCH_3	OH	H
Sinapic acid	OCH_3	OH	OCH_3

	R_1	R_2	R_3
Hydroxybenzoic acid	OH	H	H
Dihydroxybenzoic acid	OH	OH	H
Gallic acid	OH	OH	OH

	R_1	R_2	R_3
Caffeoyl quinic acid	H	Caffeic acid	H
1,3-di-*O*-Caffeoyl quinic acid	Caffeic acid	Caffeic acid	H
1,5-di-*O*-Caffeoyl quinic acid	Caffeic acid	OH	Caffeic acid

	R_1	R_2	R_3
Luteolin	H	OH	H
Quercetin	OH	OH	H
Acacetin	H	H	CH_3

Fig 8. Major classes of metabolites. Hydroxycinnamates (**A**), hydroxybenzoates (**B**), quinic acid conjugates (**C**), triterpenoid based oleanolic acid (**D**), and flavonoids (**E**), identified in *L. spinosa* extracts with selected compound(s) discussed in the text.

https://doi.org/10.1371/journal.pone.0317497.g008

viz. TNF- α, IFN-Gamma, IL-15, GSH, AST, and ALP, (Y-variables) were positioned closely to the butanol extract on the plot, indicating a strong correlation with this extract (Fig. 9A), and in agreement with biological activity parameters revealing that LS-BuOH extract exhibited the strongest activity versus LS-EtOAc and LS-EtOH extracts.

To pinpoint the MS variables strongly linked to this differentiation, metabolites with a VIP score of 5 or higher were chosen to create a correlogram, aiming to elucidate their role in biological activities. The models' validation was demonstrated by regression analysis, displaying an R2 value of 1 for all assessed parameters (Fig 9B). The correlogram (Fig 9C) indicated robust correlation among triterpenoid saponins, *i.e.*, dihydroxy-oxo-oleanenoic acid-*O*-dihexoside sulfate (peak **43**), dihydroxy-oxo-oleanenoic acid-*O*-hexosyl-rhamnoside sulfate (peak **51**), and two unknown triterpenoid saponins (peaks **53** and **59**), with correlation coefficients (R2) equal to or greater than 0.9. These correlations were observed in relation to all assessed antiparasitic activities, and infer that triterpenoidal saponins from *L. spinosa* mostly mediate for the measured bioactivities. Conversely, di-*O*-caffeoylquinic acid and hydroxylated fatty acids showed a negative correlation with the assessed antiparasitic activity parameters. There is a growing interest in triterpenoidal saponins, including their antioxidant, hepatoprotective, antiviral, and anticancer effects, as evidenced by recent studies [46–49]. This study revealed that *L. spinosa* butanol extract stands out as the most potent antiparasitic extract, primarily attributed to its rich triterpenoid saponins levels. Therefore, *L. spinosa* butanol extract may be considered for inclusion in nutraceuticals for parasite management.

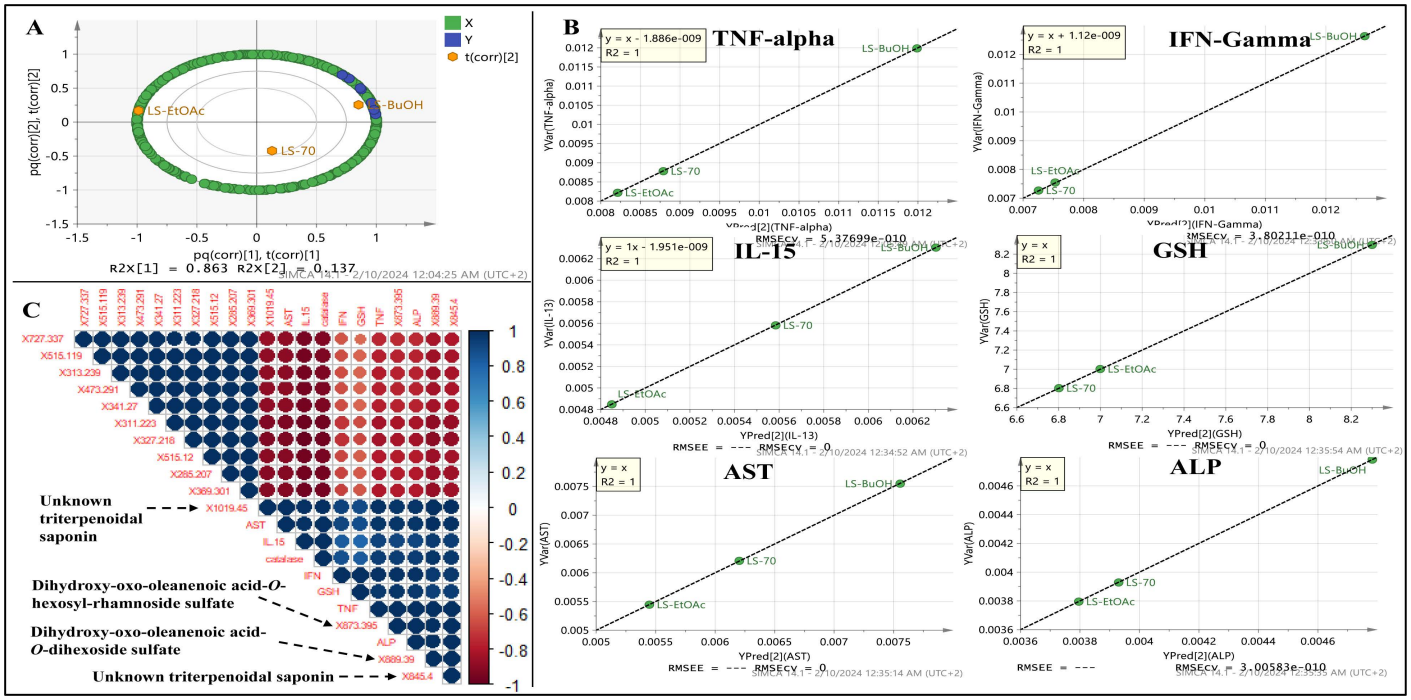

Fig 9. Partial Least Square (PLS) biplot. (**A**): PLS biplot of *L. spinosa* different extracts based on quantified metabolites by UPLC-MS negative mode designating metabolites' level as (X-variables) correlated with investigated parameters (Y-variables) related to biological assay results, (**B**): Observed versus predicted effect for biological activity parameters, i.e., TNF-alpha, IFN-Gamma, IL-15, GSH, AST, and ALP, showing correlation in relation to peaks abundance detected in negative mode. The t(corr) [2] sign denotes the correlation sites between X- and Y-variables. (**C**) Correlogram visualizing correlation between metabolites analyzed using UPLC-MS in negative mode and antiparasitic activities. The color and size of the circles are proportional to the correlation coefficients. Positive correlations are shown in blue (different shades; dark blue with the strongest correlation) whereas negative correlations in red (ranging from light red to red; dark red with the weakest correlation). (For interpretation of the references to color in this figure legend, the reader is referred to the Web version of this article).

https://doi.org/10.1371/journal.pone.0317497.g009

4. Discussion

The control of cryptosporidiosis is mostly difficult because of large numbers of oocysts excreted in the infected host feces, contaminating the surrounding environment and acting as a source of infection for humans and animals [50]. In the present study, *Cryptosporidium* spp. was isolated from diarrheic newborn buffalo calves, and the species was confirmed as *C. parvum* by PCR. This isolate was previously detected in humans and animals worldwide [51] and the human disease resembles that found in neonatal calves [52], whichis considered the most pathogenic and dominant species in farm animals [53,54]. The *C. parvum* isolate was identical to those detected in buffaloes (GenBank: ON730708.1 and ON730707.1) and cattle (GenBank: MW925062.1 and MW925061.1) from Egypt.

In the current study, the mice were used to evaluate the anti-cryptosporidial effect of three prepared *L. spinosa* extracts on *C. parvum* via assessing fecal oocyst shedding, mucosal burden, humoral and cellular immune responses in mice sera, and histopathological and immunohistochemical changes in mice intestine.

In the present study, examined mice fecal pellets revealed that mice shed many *C. parvum* oocysts from the 3rd dPI and there was a gradual decrease in oocysts' shedding in the infected-untreated mice from the 10th dPI (peak of oocyst shedding). This ensured that the infection was propagated in mice models with the selected oocysts' inoculation dose, and this coincides with previous studies which evaluated the pattern of *C. parvum* oocysts' shedding [55,56]. Herein, LS-BuOH extract reduced *C. parvum* oocysts' count significantly ($P < 0.05$) in experimentally infected mice compared to other treated groups (97% at the 10th dPI), the control group and untreated-infected mice. Similar findings were recorded in many studies using *in vitro* and *in vivo* animal models to demonstrate the effect of some plant extracts in treating diarrhea and enteritis caused by *Cryptosporidium* sp. such as: moringa [26], pomegranate peel [55], black seed [57], garlic [58,59], curcumin [60], and ginger [61]. In this study, *C. parvum* oocysts detected in infected mice were morphologically similar to other *C. parvum* shown in previous studies [26,62]. *C. parvum* oocysts in fecal pellets of LS-BuOH extract-treated mice were found to be deformed in shape, lacking inner structure, indicating that *L. spinosa* butanol extract might affect the count and infectivity of the oocysts. A similar result was recorded by Abdel Megeed [59] in a treatment trial using garlic extract against *C. parvum* in pre-weaned buffalo calves. Present results showed that *C. parvum* oocysts and developmental stages were the lowest in mice intestine of both LS-BuOH extract groups (200 mg/Kg and 100 mg/Kg; $P < 0.05$) and this might be due to the reduced severity of infection and lower parasite loads in feces in response to treatment.

Regarding humoral immune response, specific *C. parvum* antibodies IgG elevated significantly in the infected and treated mice ($P < 0.05$) at all day's post-treatment compared to the infected-untreated ones. Current findings are in accordance with other studies suggesting a significant correlation between IgG response and the intensity of infection [56,63–65]. This might be due to the release of specific antibodies during *C. parvum* infection and could be considered as a marker for cryptosporidiosis [65]. Also, the locally prepared CNBr-activated Sepharose-4B affinity purified antigen was utilized in the indirect ELISA as it had exhibited a high diagnostic potency compared to the crude antigen [8]. IgG levels were highest in the LS-BuOH extract treated group (200 mg/Kg) followed by the mice group treated with LS-BuOH extract (100 mg/Kg) compared to other treated groups. This significant effect might be due to the potential protective and immunomodulatory activity of phenolic compounds present in *L. spinosa,* especially butanol extract [18].

Modulation of the host immune response may also be relevant for selection toward commensalism, since it may prevent deleterious effects to the host resulting from the exacerbated immune response [66]. Concerning cellular immune response, levels of mice serum cytokines;

IFN-γ, IL-15 and TNF-α were significantly higher ($P < 0.001$) after 10 and 21 days of infection as compared to healthy mice. These results coincide with those of Aboelsoued et al., 2022 and Ahmad et al., 2013 [56,67], confirming that IFN-γ and IL-15 levels are important for early *C. parvum* control [68–70]. TNF-α was found to play an important role in inflammation and can be involved in protective immunity against intracellular parasites [71,72] as it regulates the growth and differentiation of a variety of cell types [73]. Robinson and his co-workers [74] assumed that TNF-α increased in cryptosporidiosis pathogenesis as it was linked with Lamnia propria histological inflammation in porcine cryptosporidiosis. Regarding IFN-γ and IL-15 levels, mice of the LS-BuOH extract treated group (200 mg/Kg) reached the maximum levels of these cytokines after 10 dPI compared to other infected groups, which then decreased towards a healthy state after 21 dPI (in which, very few oocysts appeared in fecal pellets of this mice group over the week). This might be due to reduced oocyst shedding and lower parasite loads due to the treatment, especially in the LS-BuOH extract group (200 mg/Kg). These findings agree with the association between IFN-γ and the prevention of oocyst shedding [75] and between IL-15 and control of oocyst shedding and elimination of intracellular protozoans from the intestines by activation of an NK cell-mediated pathway [76], as IL-15 is inversely correlated with *Cryptosporidium* burden [77]. In contrast, TNF-α decreased in infected mice treated with *L. spinosa* extracts with the high concentration of LS-BuOH extract at 10 and 21 dPI showcasing superiority, supportive of a role for TNF-α in inflammation which is shown to be minimal in this group after 21 dPI.

Regarding liver enzymes, a significant elevation ($P < 0.001$) in ALT, AST, and ALP in sera of *C. parvum* experimentally infected-untreated mice was detected compared to healthy mice. These findings agreed with Aboelsoued et a1. [26] and Elmahallawy et al. [78] who recorded an elevation in ALT, AST and ALP in *Cryptosporidium* experimentally infected mice. The present results indicated that cryptosporidiosis might be a major factor for severe liver injuries [79,80], hepatocellular damage mediated by *C. parvum* infection in mice [78], and confirmed the extra-intestinal effects of cryptosporidiosis [81]. This serum elevation of ALT could indicate the cell membrane injury while AST could signalize the hepatic tissue mitochondrial damage [82] and ALP could refer to hepatic cellular damage and hepatobiliary disease [83]. After 21 dPI, liver enzyme levels were significantly ($P < 0.001$) lower in mice treated with Nitazoxanide or *L. spinosa* extracts, and the best effect was observed in the LS-BuOH extract (200 mg/Kg) treated group where ALT, AST, and ALP were restored towards control healthy levels indicating the strong anti-cryptosporidial effect of LS-BuOH extract against cryptosporidiosis. This effect might be supported by previous reports in *Launaea* species which were traditionally used for the treatment of liver oxidative stress [18,84]. The determination of enzymatic antioxidant activities such as GSH–Px and catalase helps assess oxidative stress [85]. In the current study, the measured GSH–Px and catalase serum activities indicated the oxidative stress in *C. parvum* infected mice suggesting its exaggeration in response to infection [86]. These enzymes were significantly ($P < 0.001$) elevated in mice treated with Nitazoxanide or *L. spinosa* extracts with the LS-BuOH extract (200 mg/Kg) treated group showing superiority as their levels enhanced the healthy normal status, suggesting that this extract of *L. spinosa* improved mice health. This could be supported by teamwork of Abdallah [18] results that the major phenolics in *L. spinosa* showed a significant cytoprotective effect against oxidative stress which maintains the normal redox status of the cell.

In the present study, intestinal sections of *C. parvum*-infected mice showed many alterations, including lymphoplasmacytic cells infiltration, sloughing and necrosis of villi, congestion of blood vessels, and edema with the presence of *C. parvum* in the intestinal epithelium and crypt of Lieberkühn that suffered from degenerative changes. These observations fall in agreement with previous studies showing the alterations of mice intestinal tissue in response

to cryptosporidiosis [26,67,78,87,88]. The reason for this may be the impaired intestinal absorption and barrier function [89], increased paracellular permeability [90], induced innate inflammatory responses, and alteration in the tight junctions between epithelial cells [91]. These pathological alterations might be due to intestinal tissue damage with host cell death or apoptosis in response to this intracellular pathogen [92]. As a result, caspases are activated inducing apoptosis to limit the spreading of infection [93]. In the current study, there was a strong positive expression of cleaved caspase-3 as a marker of infection-induced apoptosis in the intestinal sections of the *C. parvum* infected-untreated mice group. These results matched with Aboelsoued et al. [35], revealing that Caspase-3 was highly expressed in the intestine of *C. parvum*-infected mice, as well as results from Sasahara [94] and Buret [95], suggesting that this epithelial apoptosis could be integral for *C. parvum* pathogenicity and could promote host cell apoptosis. Meanwhile, mice treated with Nitazoxanide and *L. spinosa* extracts showed enhancement of histological characteristics of the intestinal tissue and caspase-3 expression with a marked amelioration in both doses of LS-BuOH extract (100 and 200 mg/Kg). Restoration of the histopathological alterations in intestinal architectures and caspase-3 expression after treatment with *L. spinosa* extracts was significant and was matched with lower mucosal burden and other immunological, biochemical, and inflammatory markers.

With regards to natural product classes reported to exhibit anti-parasitic effects, saponins were found to play a significant role in the *in vitro* inhibition of *C. parvum* oocyst growth [96]. EL-Shewehy et al [97] reported that extracts of *Zingiber officinale*, *Allium sativum*, and *Punica granatum* exert significant anti-cryptosporidium potencies due to the high contents of saponins along with flavonoids and phenolics. According to reports, saponins' anti-cryptosporidium mechanism of action involves disrupting the protozoal membrane, deactivating enzymes, and depriving cells of materials and metal ions that are essential to cell metabolism [98,99]. El-Sayed and Fathy additionally found that saponins significantly contributed to anti-*Cryptosporidium* impacts through interference with lectin receptors. The potential of *Allium cepa* extract to significantly lower the number of *C. parvum* oocysts has also been associated with flavonoids and sulfated substances [100]. The current chemical profiling of the three extracts of *L. spinosa*, LS-EtOAc, LS-EtOH and LS-BuOH, revealed an abundance of triterpenoid saponins, phenolic acids, and flavonoid conjugates. All these compounds were demonstrated to exhibit strong antioxidant and anti-inflammatory actions [101]. These phenolic and flavonoid components are exogenous antioxidant mediators that function by blocking ion channels, nitric oxide synthase, and xanthine oxide synthase [102], in addition to showcasing antioxidant effects. For example, it was shown that apigenin, luteolin, and their derivatives, as strong antioxidant components, decreased the expression of caspase-3 and other indicators of oxidative stress, including glutathione peroxidase, malondialdehyde, and superoxide dismutase [103]. Phenolics and flavonoids in parsley and dill plants decreased Reactive oxygen species (ROS) levels. Additionally, they strengthen the antioxidant enzyme glutathione-S-transferase (GST) [104]. Partial Least Square correlation results confirmed the significant roles of the triterpenoid saponins, and were in full agreement with previous studies confirming their antioxidant, anti-inflammatory, and antiviral effects [105,106]. Triterpenoid saponins disrupt oocyst formation and prevent parasite sporulation. Sulfated triterpenoidal saponins have garnered attention for their broad spectrum of biological activities, including their antiparasitic potential [105,106]. This property is crucial when considering *Cryptosporidium* treatment, as the parasite's life cycle involves stages, such as oocysts and sporozoites, that are protected by robust membrane structures. Saponins, particularly those that are sulfated, have demonstrated the ability to disrupt cell membranes, leading to parasite lysis and death, thus reducing infection severity.

While previous studies have reported the antiparasitic potential of plant-derived saponins, sulfated triterpenoidal saponins may offer a distinctive advantage due to their enhanced water solubility and bioavailability. This can potentially improve their interaction with *Cryptosporidium* at different life stages, especially during the intestinal sporozoite invasion. Additionally, their ability to modulate host immune responses, stimulate mucosal immunity, and act as adjuvants could provide a dual mechanism of action—both directly attacking the parasite while also enhancing the host's defenses. To further differentiate this study, it would be essential to investigate whether the sulfation pattern influences saponin activity against *Cryptosporidium*, which could highlight a unique therapeutic mechanism compared to other non-sulfated saponins documented in existing literature.

Conclusion

Annually, gastrointestinal cases and waterborne disease outbreaks are primarily brought about by *C. parvum* throughout the globe. *L. spinosa* has traditionally been employed to treat several diseases including gastrointestinal diseases. Fecal *C. parvum* oocyst count and mucosal load were decreased by *L. spinosa* extracts. The levels of IgG, IFN-γ, and IL-15 along with TNF-α were all restored to a healthy state. Additionally, upon extract administration, levels of liver enzymes were reduced while GSH-Px and catalase rose. The histo- and immunohistopathological findings, which demonstrated that *L. spinosa* extracts reduced cleaved caspase-3, damage score, and degenerative alterations expressions, corroborate the above findings. Herein, the anti-cryptosporidial potency of the three extracts of *L. spinosa* was evaluated and found to be most effective in the following order: LS-BuOH> LS-EtOH> LS-EtOAc. This study reports the presence of sulfated triterpenoid saponins in *Launaea* genus for the first time in the literature, alongside several other new metabolites. Biological effects were shown to be strongly related to LS-BuOH extract (R2: 0.9) according to PLS regression analysis, with triterpenoid saponins and flavonoid glycosides primarily responsible for the anti-parasitic effect. The outcomes of the present study suggest that *L. spinosa* extracts could be an innovative therapy for *C. parvum* management yet to be tested in clinical trials.

Supporting information

S1 File. Fig. S1 ESI-MS/MS spectrum of peak **10**, **17**, **18**, and **21** in the negative ion mode. Fig. S2 ESI-MS/MS spectrum of peak **26**, **37**, and **42** in the negative ion mode. Fig. S3 ESI-MS/MS spectrum of peak **8** and **12** in the negative ion mode. Fig. S4 ESI-MS/MS spectrum of peak **2** in the negative ion mode. Fig. S5 ESI-MS/MS spectrum of peak **34** in the negative ion mode. Fig. S6 ESI-MS/MS spectrum of peak **33** in the negative ion mode. Fig. S7 ESI-MS/MS spectrum of peak **56** in the negative ion mode. Fig. S8 ESI-MS/MS spectrum of peak **47** in the negative ion mode. Fig. S9 ESI-MS/MS spectrum of peak **68** in the negative ion mode. Fig. S10 ESI-MS/MS spectrum of peak **67** in the negative ion mode.
(DOCX)

S1 Raw data. Launea Crypto *Raw data.xlsx* The raw data of (i) Reduction % in C . *parvum* oocysts' shedding, (ii) Serum IgG level, (iii) Serum INF-γ, IL-15 and TNF-α levels, (iv) Serum liver function parameters (ALT, AST and ALP), and (v) Antioxidant activity parameters (GSH-Px and Catalase).
(XLSX)

Acknowledgment

The authors thank Dr. Patrick Elliott, Human Nutrition, UCD Institute of Food and Health, Dublin, Ireland for proofreading the manuscript and for language correction.

Author contributions

Conceptualization: Mohamed A. Farag, Abdelsamed Elshamy.

Data curation: Dina Aboelsoued, Mohamed A. Farag, Abdelsamed Elshamy, Abdelbaset M. Elgamal.

Formal analysis: Mohamed G. Sharaf El-Din, Dina Aboelsoued, Mohamed F. Abdelhameed, Mohamed A. El-Saied, Mohamed A. Farag, Abdelsamed Elshamy.

Investigation: Mai M. Elghonemy, Mohamed G. Sharaf El-Din, Dina Aboelsoued, Mohamed F. Abdelhameed, Mohamed A. El-Saied, Nagwa I. Toaleb, Mohamed A. Farag, Abdelsamed Elshamy, Abdelbaset M. Elgamal.

Methodology: Mai M. Elghonemy, Mohamed G. Sharaf El-Din, Dina Aboelsoued, Mohamed F. Abdelhameed, Mohamed A. El-Saied, Nagwa I. Toaleb, Mohamed A. Farag, Abdelsamed Elshamy, Abdelbaset M. Elgamal.

Software: Dina Aboelsoued.

Writing – original draft: Mai M. Elghonemy, Mohamed G. Sharaf El-Din, Dina Aboelsoued, Mohamed F. Abdelhameed, Mohamed A. El-Saied, Mohamed A. Farag, Abdelsamed Elshamy, Abdelbaset M. Elgamal.

Writing – review & editing: Mai M. Elghonemy, Dina Aboelsoued, Mohamed F. Abdelhameed, Mohamed A. El-Saied, Mohamed A. Farag, Abdelbaset M. Elgamal.

References

1. Widmer G, Carmena D, Kváč M, Chalmers RM, Kissinger JC, Xiao L, et al. Update on cryptosporidium spp.: highlights from the seventh international giardia and cryptosporidium conference. Parasite. 2020;2714. https://doi.org/10.1051/parasite/2020011 PMID: 32167464
2. Ebiyo A, Haile G. Prevalence and factors associated with cryptosporidium infection in calves in and around nekemte town, east wollega zone of ethiopia. Vet Med Int. 2022;20221468242. https://doi.org/10.1155/2022/1468242 PMID: 35222937
3. Gharpure R, Perez A, Miller AD, Wikswo ME, Silver R, Hlavsa MC. Cryptosporidiosis Outbreaks—United States, 2009-2017. MMWR Morb Mortal Wkly Rep. 2019;68(25):568–72. https://doi.org/10.15585/mmwr.mm6825a3 PMID: 31246941
4. Ryan U, Hijjawi N, Xiao L. Foodborne cryptosporidiosis. Int J Parasitol. 2018;48(1):1–12. https://doi.org/10.1016/j.ijpara.2017.09.004 PMID: 29122606
5. Helmy YA, Hafez HM. Cryptosporidiosis: from prevention to treatment, a narrative review. Microorganisms. 2022;10(12):2456. https://doi.org/10.3390/microorganisms10122456 PMID: 36557709
6. Hatam-Nahavandi K, Ahmadpour E, Carmena D, Spotin A, Bangoura B, Xiao L. Cryptosporidium infections in terrestrial ungulates with focus on livestock: a systematic review and meta-analysis. Parasit Vectors. 2019;12(1):453. https://doi.org/10.1186/s13071-019-3704-4 PMID: 31521186
7. Tzipori S. Cryptosporidiosis in perspective. Adv Parasitol. 1988;27:63–129. https://doi.org/10.1016/s0065-308x(08)60353-x PMID: 3289331
8. Aboelsoued D, Abdel Megeed KN. Diagnosis and control of cryptosporidiosis in farm animals. J Parasit Dis. 2022;46(4):1133–46. https://doi.org/10.1007/s12639-022-01513-2 PMID: 36457776
9. Mammeri M, Chevillot A, Thomas M, Polack B, Julien C, Marden J-P, et al. Efficacy of chitosan, a natural polysaccharide, against Cryptosporidium parvum in vitro and in vivo in neonatal mice. Exp Parasitol. 2018;1941–8. https://doi.org/10.1016/j.exppara.2018.09.003 PMID: 30237052
10. Santin M. Cryptosporidium and giardia in ruminants. Vet Clin North Am Food Anim Pract. 2020;36(1):223–38. https://doi.org/10.1016/j.cvfa.2019.11.005 PMID: 32029186
11. Brainard J, Hammer CC, Hunter PR, Katzer F, Hurle G, Tyler K. Efficacy of halofuginone products to prevent or treat cryptosporidiosis in bovine calves: a systematic review and meta-analyses. Parasitology. 2021;148(4):408–19. https://doi.org/10.1017/S0031182020002267 PMID: 33261668
12. Elshamy AI, Abd-ElGawad AM, El-Amier YA, El Gendy AEG, Al-Rowaily SL. Interspecific variation, antioxidant and allelopathic activity of the essential oil from three Launaea species growing naturally in heterogeneous habitats in Egypt. Flavour & Fragrance J. 2019;34(5):316–28. https://doi.org/10.1002/ffj.3512

13. El-Fadaly AA, Younis IY, Abdelhameed MF, Ahmed YH, Ragab TIM, El Gendy AE-NG, et al. Protective action mechanisms of launaea mucronata extract and its nano-formulation against nephrotoxicity in rats as revealed via biochemical, histopathological, and UPLC-QTOF-MS/MS Analyses. Metabolites. 2023;13(7):786. https://doi.org/10.3390/metabo13070786 PMID: 37512493

14. Makasana A, Ranpariya V, Desai D, Mendpara J, Parekh V. Evaluation for the anti-urolithiatic activity of Launaea procumbens against ethylene glycol-induced renal calculi in rats. Toxicol Rep. 2014;146–52. https://doi.org/10.1016/j.toxrep.2014.03.006 PMID: 28962225

15. Khan RA, Khan MR, Sahreen S, Ahmed M. Assessment of flavonoids contents and in vitro antioxidant activity of Launaea procumbens. Chem Cent J. 2012;6(1):43. https://doi.org/10.1186/1752-153X-6-43 PMID: 22616896

16. Qureshi S, Awan A, Khan M, Bano S. Taxonomic study of the genus Launaea L. from Pakistan. Online J Biol Sci. 2002;2315–9.

17. Cheriti A, Belboukhari M, Belboukhari N, Djeradi H. Phytochemical and biological studies on Launaea Cass. genus (Asteraceae) from Algerian Sahara. Phytochemistry. 2012;11: 67–80.

18. Abdallah H, Farag M, Osman S, Kim D hye, Kang K, Pan C-H, et al. Isolation of major phenolics from Launaea spinosa and their protective effect on HepG2 cells damaged with t-BHP. Pharm Biol. 2016;54(3):536–41. https://doi.org/10.3109/13880209.2015.1052885 PMID: 26052623

19. Asif M, , Saadullah M, Yaseen HS, Saleem M, Yousaf HM, et al. Evaluation of in vivo anti-inflammatory and anti-angiogenic attributes of methanolic extract of Launaea spinosa. Inflammopharmacology. 2020;28(4):993–1008. https://doi.org/10.1007/s10787-020-00687-6 PMID: 32172496

20. Henriksen SA, Pohlenz JF. Staining of cryptosporidia by a modified Ziehl-Neelsen technique. Acta Vet Scand. 1981;22(3–4):594–6. https://doi.org/10.1186/BF03548684 PMID: 6178277

21. Heine J. A simple technic for the demonstration of cryptosporidia in feces. Zentralbl Veterinarmed B. 1982;29(4):324–7. https://doi.org/10.1111/j.1439-0450.1982.tb01233.x PMID: 6181632

22. Current WL, Reese NC. A comparison of endogenous development of three isolates of Cryptosporidium in suckling mice. J Protozool. 1986;33(1):98–108. https://doi.org/10.1111/j.1550-7408.1986.tb05567.x PMID: 3959014

23. Feltus DC, Giddings CW, Schneck BL, Monson T, Warshauer D, McEvoy JM. Evidence supporting zoonotic transmission of Cryptosporidium spp. in Wisconsin. J Clin Microbiol. 2006;44(12):4303–8. https://doi.org/10.1128/JCM.01067-06 PMID: 17005736

24. Thompson JD, Higgins DG, Gibson TJ. CLUSTAL W: improving the sensitivity of progressive multiple sequence alignment through sequence weighting, position-specific gap penalties and weight matrix choice. Nucleic Acids Res. 1994;22(22):4673–80. https://doi.org/10.1093/nar/22.22.4673 PMID: 7984417

25. Tamura K, Stecher G, Peterson D, Filipski A, Kumar S. MEGA6: molecular evolutionary genetics analysis version 6.0. Mol Biol Evol. 2013;30(12):2725–9. https://doi.org/10.1093/molbev/mst197 PMID: 24132122

26. Aboelsoued D, Abo-Aziza FAM, Mahmoud MH, Abdel Megeed KN, Abu El Ezz NMT, Abu-Salem FM. Anticryptosporidial effect of pomegranate peels water extract in experimentally infected mice with special reference to some biochemical parameters and antioxidant activity. J Parasit Dis. 2019;43(2):215–28. https://doi.org/10.1007/s12639-018-01078-z PMID: 31263326

27. Kaushik K, Khurana S, Wanchu A, Malla N. Serum immunoglobulin G, M and A response to Cryptosporidium parvum in Cryptosporidium-HIV co-infected patients. BMC Infect Dis. 2009;9179. https://doi.org/10.1186/1471-2334-9-179 PMID: 19922628

28. LOWRY OH, ROSEBROUGH NJ, FARR AL, RANDALL RJ. Protein measurement with the Folin phenol reagent. J Biol Chem. 1951;193(1):265–75. https://doi.org/10.1016/s0021-9258(19)52451-6 PMID: 14907713

29. Fagbemi BO, Obarisiagbon IO, Mbuh JV. Detection of circulating antigen in sera of Fasciola gigantica-infected cattle with antibodies reactive with a Fasciola-specific 88-kDa antigen. Vet Parasitol. 1995;58(3):235–46. https://doi.org/10.1016/0304-4017(94)00718-r PMID: 7571328

30. Aboelsoued D, Hendawy S, Abdullah H, Abdel Megeed K, Hassan S, El Hakim A, et al. Diagnosis of cryptosporidiosis using affinity purified antigen. Egyptian Journal of Veterinary Sciences. 2022;53(3):459–73. https://doi.org/10.21608/ejvs.2022.145814.1354

31. Ortolani EL. Standardization of the modified Ziehl-Neelsen technique to stain oocysts of Cryptosporidium sp. Rev Bras Parasitol Veterinária. n.d.;929–31.

32. Farid A, Tawfik A, Elsioufy B, Safwat G. In vitro and in vivo anti-Cryptosporidium and anti-inflammatory effects of Aloe vera gel in dexamethasone immunosuppressed mice. Int J Parasitol Drugs Drug Resist. 2021;17: 156–67. https://doi.org/10.1016/j.ijpddr.2021.09.002

33. Priest JW, Kwon JP, Moss DM, Roberts JM, Arrowood MJ, Dworkin MS, et al. Detection by enzyme immunoassay of serum immunoglobulin G antibodies that recognize specific Cryptosporidium parvum antigens. J Clin Microbiol. 1999;37(5):1385–92. https://doi.org/10.1128/JCM.37.5.1385-1392.1999 PMID: 10203492

34. Oriá RB, Costa DVS, de Medeiros PHQS, Roque CR, Dias RP, Warren CA, et al. Myeloperoxidase as a biomarker for intestinal-brain axis dysfunction induced by malnutrition and Cryptosporidium infection in weanling mice. Braz J Infect Dis. 2023;27(3):102776. https://doi.org/10.1016/j.bjid.2023.102776 PMID: 37150212

35. Aboelsoued D, Toaleb NI, Ibrahim S, Shaapan RM, Megeed KNA. A Cryptosporidium parvum vaccine candidate effect on immunohistochemical profiling of CD4+, CD8+, Caspase-3 and NF-κB in mice. BMC Vet Res. 2023;19(1):216. https://doi.org/10.1186/s12917-023-03699-w PMID: 37858196

36. Farrag ARH, Abdallah HMI, Khattab AR, Elshamy AI, Gendy AE-NGE, Mohamed TA, et al. Antiulcer activity of Cyperus alternifolius in relation to its UPLC-MS metabolite fingerprint: A mechanistic study. Phytomedicine. 2019;62:152970. https://doi.org/10.1016/j.phymed.2019.152970 PMID: 31181403

37. Abdel Shakour ZT, El-Akad RH, Elshamy AI, El Gendy AE-NG, Wessjohann LA, Farag MA. Dissection of Moringa oleifera leaf metabolome in context of its different extracts, origin and in relationship to its biological effects as analysed using molecular networking and chemometrics. Food Chem. 2023;399:133948. https://doi.org/10.1016/j.foodchem.2022.133948 PMID: 35994855

38. Farag MA, Sharaf El-Din MG, Aboul-Fotouh Selim M, Owis AI, Abouzid SF. Mass spectrometry-based metabolites profiling of nutrients and anti-nutrients in major legume sprouts. Food Bioscience. 2021;39:100800. https://doi.org/10.1016/j.fbio.2020.100800

39. Farag MA, El-Ahmady SH, Elian FS, Wessjohann LA. Metabolomics driven analysis of artichoke leaf and its commercial products via UHPLC-q-TOF-MS and chemometrics. Phytochemistry. 2013;95:177–87. https://doi.org/10.1016/j.phytochem.2013.07.003 PMID: 23902683

40. Wishart DS, Guo A, Oler E, Wang F, Anjum A, Peters H, et al. HMDB 5.0: the human metabolome database for 2022. Nucleic Acids Res. 2022;50(D1):D622–31. https://doi.org/10.1093/nar/gkab1062 PMID: 34986597

41. Davis BD, Brodbelt JS. Determination of the glycosylation site of flavonoid monoglucosides by metal complexation and tandem mass spectrometry. J Am Soc Mass Spectrom. 2004;15(9):1287–99. https://doi.org/10.1016/j.jasms.2004.06.003 PMID: 15337509

42. Pradas Del Real AE, Silvan JM, de Pascual-Teresa S, Guerrero A, García-Gonzalo P, Lobo MC, et al. Role of the polycarboxylic compounds in the response of Silene vulgaris to chromium. Environ Sci Pollut Res Int. 2017;24(6):5746–56. https://doi.org/10.1007/s11356-016-8218-4 PMID: 28050761

43. Mroczek A, Kapusta I, Stochmal A, Janiszowska W. MS/MS and UPLC-MS profiling of triterpenoid saponins from leaves and roots of four red beet (Beta vulgaris L.) cultivars. Phytochem Lett. 2019;30333–7. https://doi.org/10.1016/j.phytol.2019.02.015

44. Kleinenkuhnen N, Büchel F, Gerlich SC, Kopriva S, Metzger S. A novel method for identification and quantification of sulfated flavonoids in plants by neutral loss scan mass spectrometry. Front Plant Sci. 2019;10885. https://doi.org/10.3389/fpls.2019.00885 PMID: 31333712

45. Farag MA, Rasheed DM, Kropf M, Heiss AG. Metabolite profiling in Trigonella seeds via UPLC-MS and GC-MS analyzed using multivariate data analyses. Anal Bioanal Chem. 2016;408(28):8065–78. https://doi.org/10.1007/s00216-016-9910-4 PMID: 27614978

46. Simões CM, Amoros M, Girre L. Mechanism of antiviral activity of triterpenoid saponins. Phytother Res. 1999;13(4):323–8. https://doi.org/10.1002/(SICI)1099-1573(199906)13:4<323::AID-PTR448>3.0.CO;2-C PMID: 10404540

47. Huang B, Fu H-Z, Chen W-K, Luo Y-H, Ma S-C. Hepatoprotective triterpenoid saponins from Callicarpa nudiflora. Chem Pharm Bull (Tokyo). 2014;62(7):695–9. https://doi.org/10.1248/cpb.c14-00159 PMID: 24804828

48. Liu Y-Y, Yang Y-N, Feng Z-M, Jiang J-S, Zhang P-C. Eight new triterpenoid saponins with antioxidant activity from the roots of Glycyrrhiza uralensis Fisch. Fitoterapia. 2019;133186–92. https://doi.org/10.1016/j.fitote.2019.01.014 PMID: 30690123

49. Elekofehinti OO, Iwaloye O, Olawale F, Ariyo EO. Saponins in cancer treatment: current progress and future prospects. Pathophysiology. 2021;28(2):250–72. https://doi.org/10.3390/pathophysiology28020017 PMID: 35366261

50. Khan SM, Witola WH. Past, current, and potential treatments for cryptosporidiosis in humans and farm animals: a comprehensive review. Front Cell Infect Microbiol. 2023;131115522. https://doi.org/10.3389/fcimb.2023.1115522 PMID: 36761902

51. Ryan U, Zahedi A, Feng Y, Xiao L. An update on zoonotic cryptosporidium species and genotypes in humans. Animals (Basel). 2021;11(11):3307. https://doi.org/10.3390/ani11113307 PMID: 34828043

52. Santín M, Trout JM. Livestock. Cryptosporidium and cryptosporidiosis. CRC Press; 2007. pp. 451–484.

53. Singh BB, Sharma R, Kumar H, Banga HS, Aulakh RS, Gill JPS, et al. Prevalence of Cryptosporidium parvum infection in Punjab (India) and its association with diarrhea in neonatal dairy calves. Vet Parasitol. 2006;140(1–2):162–5. https://doi.org/10.1016/j.vetpar.2006.03.029 PMID: 16647820

54. Huang Y, Song Y, You Y, Mi R, Han X, Gong H, et al. Development of an immunocompetent mouse model susceptible to Cryptosporidium tyzzeri infection. Parasite Immunol. 2021;43(1):e12800. https://doi.org/10.1111/pim.12800 PMID: 33068486

55. Al-Mathal EM, Alsalem AM. Pomegranate (Punica granatum) peel is effective in a murine model of experimental Cryptosporidium parvum. Exp Parasitol. 2012;131(3):350–7. https://doi.org/10.1016/j.exppara.2012.04.021 PMID: 22580265

56. Aboelsoued D, Abdullah HHAM, Megeed KNA, Hassan SE, Toaleb NI. Evaluation of a vaccine candidate isolated from Cryptosporidium parvum oocyst in mice. Vet World. 2022;15(12):2772–84. https://doi.org/10.14202/vetworld.2022.2772-2784 PMID: 36718331

57. Ahmad A, Husain A, Mujeeb M, Khan SA, Najmi AK, Siddique NA, et al. A review on therapeutic potential of Nigella sativa: a miracle herb. Asian Pac J Trop Biomed. 2013;3(5):337–52. https://doi.org/10.1016/S2221-1691(13)60075-1 PMID: 23646296

58. Toulah FH, El-Shafei AA, Al-Rashidi HS. Evaluation of garlic plant and indinavir drug efficacy in the treatment of cryptosporidiosis in experimentally immumosuppressed rats. J Egypt Soc Parasitol. 2012;42(2):321–8. https://doi.org/10.12816/0006320 PMID: 23214211

59. Megeed KNA, Hammam AM, Morsy GH, Khalil FAM, Seliem MME, Aboelsoued D. Control of cryptosporidiosis in buffalo calves using garlic (Allium sativum) and nitazoxanide with special reference to some biochemical parameters. Global Veterinaria. 2015;14:646–55.

60. Asadpour M, Namazi F, Razavi SM, Nazifi S. Curcumin: A promising treatment for Cryptosporidium parvum infection in immunosuppressed BALB/c mice. Exp Parasitol. 2018;195:59–65. https://doi.org/10.1016/j.exppara.2018.10.008 PMID: 30385266

61. Abouelsoued D, Shaapan R, Elkhateeb RM, Elnattat W, Abd elhameed mohamed, Hammam AMM, et al. Therapeutic Efficacy of Ginger (Zingiber officinale), Ginseng (Panax ginseng) and Sage (Salvia officinalis) Against Cryptosporidium parvum in Experimentally Infected Mice. NIDOC-ASRT. 2020;51(2):241–51. https://doi.org/10.21608/ejvs.2020.24183.1152

62. Abdelrahman KA, Abdel Megeed KN, Hammam AM, Morsy GH, Seliem MME, Aboelsoued D. Molecular characterization of bubaline isolate of Cryptosporidium species from Egypt. Res J Parasit. 2015;10:127–41.

63. El Shazly AMA, Soltan DM, El-Sheikha HM, Sadek GS, Morsy ATA. Correlation of ELISA coproantigen and oocysts count to the severity of cryptosporidiosis parvum in children. J Egypt Soc Parasitol. 2007;37(1):107–20. PMID: 17580571

64. Yu J-R, Lee S-U. Time gap between oocyst shedding and antibody responses in mice infected with Cryptosporidium parvum. Korean J Parasitol. 2007;45(3):225–8. https://doi.org/10.3347/kjp.2007.45.3.225 PMID: 17876169

65. Jakobi V, Petry F. Humoral immune response in IL-12 and IFN-gamma deficient mice after infection with Cryptosporidium parvum. Parasite Immunol. 2008;30(3):151–61. https://doi.org/10.1111/j.1365-3024.2007.01013.x PMID: 18179628

66. Rossi A, Marqués JM, Gavidia CM, Gonzalez AE, Carmona C, García HH, et al. Echinococcus granulosus: different cytokine profiles are induced by single versus multiple experimental infections in dogs. Exp Parasitol. 2012;130(2):110–5. https://doi.org/10.1016/j.exppara.2011.12.006 PMID: 22202182

67. Allam NAT, Hamouda RAE-F, Sedky D, Abdelsalam ME, El-Gawad MEHA, Hassan NMF, et al. Medical prospects of cryptosporidiosis in vivo control using biofabricated nanoparticles loaded with Cinnamomum camphora extracts by Ulva fasciata. Vet World. 2024;17(1):108–24. https://doi.org/10.14202/vetworld.2024.108-124 PMID: 38406364

68. El-Wakil ES, Salem AE, Al-Ghandour AMF. Evaluation of possible prophylactic and therapeutic effect of mefloquine on experimental cryptosporidiosis in immunocompromised mice. J Parasit Dis. 2021;45(2):380–93. https://doi.org/10.1007/s12639-020-01315-4 PMID: 34295037

69. Gullicksrud JA, Sateriale A, Engiles JB, Gibson AR, Shaw S, Hutchins ZA, et al. Enterocyte-innate lymphoid cell crosstalk drives early IFN-γ-mediated control of cryptosporidium. Mucosal Immunol. 2022;15(2):362–72. https://doi.org/10.1038/s41385-021-00468-6 PMID: 34750455

70. Chang L, Chen Y, Kang Q, Qin J, Liu Z. Detection of expression alteration of cytokines in the intestine of Balb/c mice infected with Cryptosporidium parvum using relative fluorescence quantitative PCR method. Pakistan Journal of Zoology. n.d.;54.

71. Zganiacz A, Santosuosso M, Wang J, Yang T, Chen L, Anzulovic M, et al. TNF-alpha is a critical negative regulator of type 1 immune activation during intracellular bacterial infection. J Clin Invest. 2004;113(3):401–13. https://doi.org/10.1172/JCI18991 PMID: 14755337

72. Lean I-S, Lacroix-Lamandé S, Laurent F, McDonald V. Role of tumor necrosis factor alpha in development of immunity against Cryptosporidium parvum infection. Infect Immun. 2006;74(7):4379–82. https://doi.org/10.1128/IAI.00195-06 PMID: 16790816

73. Ahmed SR, Mostafa EM, Musa A, Rateb EE, Al-Sanea MM, Abu-Baih DH, et al. Wound healing and antioxidant properties of launaea procumbens supported by metabolomic profiling and molecular docking. Antioxidants (Basel). 2022;11(11):2258. https://doi.org/10.3390/antiox11112258 PMID: 36421445

74. Kandil HM, Berschneider HM, Argenzio RA. Tumour necrosis factor alpha changes porcine intestinal ion transport through a paracrine mechanism involving prostaglandins. Gut. 1994;35(7):934–40. https://doi.org/10.1136/gut.35.7.934 PMID: 8063221

75. White AC, Robinson P, Okhuysen PC, Lewis DE, Shahab I, Lahoti S, et al. Interferon-gamma expression in jejunal biopsies in experimental human cryptosporidiosis correlates with prior sensitization and control of oocyst excretion. J Infect Dis. 2000;181(2):701–9. https://doi.org/10.1086/315261 PMID: 10669358

76. Dann SM, Wang H-C, Gambarin KJ, Actor JK, Robinson P, Lewis DE, et al. Interleukin-15 activates human natural killer cells to clear the intestinal protozoan cryptosporidium. J Infect Dis. 2005;192(7):1294–302. https://doi.org/10.1086/444393 PMID: 16136475

77. Kothavade RJ. Challenges in understanding the immunopathogenesis of Cryptosporidium infections in humans. Eur J Clin Microbiol Infect Dis. 2011;30(12):1461–72. https://doi.org/10.1007/s10096-011-1246-6 PMID: 21484252

78. Elmahallawy EK, Elshopakey GE, Saleh AA, Agil A, El-Morsey A, El-Shewehy DMM, et al. S-Methylcysteine (SMC) ameliorates intestinal, hepatic, and splenic damage induced by cryptosporidium parvum infection via targeting inflammatory modulators and oxidative stress in swiss albino mice. Biomedicines. 2020;8(10):423. https://doi.org/10.3390/biomedicines8100423 PMID: 33076496

79. Wasmuth HE, Kunz D, Yagmur E, Timmer-Stranghöner A, Vidacek D, Siewert E, et al. Patients with acute on chronic liver failure display "sepsis-like" immune paralysis. J Hepatol. 2005;42(2):195–201. https://doi.org/10.1016/j.jhep.2004.10.019 PMID: 15664244

80. Mousa N, Abdel-Razik A, El-Nahas H, El-Shazly A, Abdelaziz M, Nabih M. Cryptosporidiosis in patients with diarrhea and chronic liver diseases. J Infect Dev Count. 2014;8:1584–90.

81. Chalmers RM, Davies AP. Minireview: clinical cryptosporidiosis. Exp Parasitol. 2010;124(1):138–46. https://doi.org/10.1016/j.exppara.2009.02.003 PMID: 19545516

82. AbouGabal A, Aboul-Ela HM, Ali E, Khaled AEM, Shalaby OK. Hepatoprotective, DNA damage prevention and antioxidant potential of Spirulina platensis on CCl4-induced hepatotoxicity in mice. Am J Biomed Res. 2015;3:29–34.

83. Fernandes M da S, Iano FG, Rocia V, Yanai MM, Leite A de L, Furlani TA, et al. Alkaline phosphatase activity in plasma and liver of rats submitted to chronic exposure to fluoride. Braz arch biol technol. 2011;54(6):1187–92. https://doi.org/10.1590/s1516-89132011000600014

84. Khidr Z, Ebad F, El-Khawaga H. Osmoregulation and antimicrobial activity of two egyptian true xerophytes; launaea spinosa (forssk.) And leptadenia pyrotechnica (forssk.). Egypt J Desert Res. 2017;67(2):331–49. https://doi.org/10.21608/ejdr.2017.21132

85. Saleh MA, Mahran OM, Bassam Al-Salahy M. Circulating oxidative stress status in dromedary camels infested with sarcoptic mange. Vet Res Commun. 2011;35(1):35–45. https://doi.org/10.1007/s11259-010-9450-x PMID: 21082344

86. Abo-Aziza F, Hendawy S, Abd El-Kader Z, Oda S, El-Namaky A. Clinicohistopathological and immunological alterations in egyptian donkeys infested by rhinoestrus spp. during the winter season. NIDOC-ASRT. 2017;48(2):61–71. https://doi.org/10.21608/ejvs.2017.1555.1019

87. Shahbazi P, Nematollahi A, Arshadi S, Farhang HH, Shahbazfar AA. The protective effect of artemisia spicigera ethanolic extract against cryptosporidium parvum infection in immunosuppressed mice. Iran J Parasitol. 2021;16(2):279–88. https://doi.org/10.18502/ijpa.v16i2.6318 PMID: 34557243

88. Soufy H, El-Beih NM, Nasr SM, Abd El-Aziz TH, Khalil FAM, Ahmed YF, et al. Effect of Egyptian propolis on cryptosporidiosis in immunosuppressed rats with special emphasis on oocysts shedding, leukogram, protein profile and ileum histopathology. Asian Pac J Trop Med. 2017;10(3):253–62. https://doi.org/10.1016/j.apjtm.2017.03.004 PMID: 28442108

89. Di Genova BM, Tonelli RR. Infection strategies of intestinal parasite pathogens and host cell responses. Front Microbiol. 2016;7256. https://doi.org/10.3389/fmicb.2016.00256 PMID: 26973630

90. Klein P, Kleinová T, Volek Z, Simůnek J. Effect of Cryptosporidium parvum infection on the absorptive capacity and paracellular permeability of the small intestine in neonatal calves. Vet Parasitol. 2008;152(1–2):53–9. https://doi.org/10.1016/j.vetpar.2007.11.020 PMID: 18248900

91. Mead JR. Prospects for immunotherapy and vaccines against Cryptosporidium. Hum Vaccin Immunother. 2014;10(6):1505–13. https://doi.org/10.4161/hv.28485 PMID: 24638018

92. McCole DF, Eckmann L, Laurent F, Kagnoff MF. Intestinal epithelial cell apoptosis following Cryptosporidium parvum infection. Infect Immun. 2000;68(3):1710–3. https://doi.org/10.1128/IAI.68.3.1710-1713.2000 PMID: 10678994

93. Uchiyama R, Tsutsui H. Caspases as the key effectors of inflammatory responses against bacterial infection. Arch Immunol Ther Exp (Warsz). 2015;63(1):1–13. https://doi.org/10.1007/s00005-014-0301-2 PMID: 25033773

94. Sasahara T, Maruyama H, Aoki M, Kikuno R, Sekiguchi T, Takahashi A, et al. Apoptosis of intestinal crypt epithelium after Cryptosporidium parvum infection. J Infect Chemother. 2003;9(3):278–81. https://doi.org/10.1007/s10156-003-0259-1 PMID: 14513402

95. Buret AG, Chin AC, Scott KGE. Infection of human and bovine epithelial cells with Cryptosporidium andersoni induces apoptosis and disrupts tight junctional ZO-1: effects of epidermal growth factor. Int J Parasitol. 2003;33(12):1363–71. https://doi.org/10.1016/s0020-7519(03)00138-3 PMID: 14527519

96. Ranasinghe S, Zahedi A, Armson A, Lymbery AJ, Ash A. In vitro susceptibility of cryptosporidium parvum to plant antiparasitic compounds. Pathogens. 2022;12(1):61. https://doi.org/10.3390/pathogens12010061 PMID: 36678409

97. El-Shewehy DMM, Elshopakey GE, Ismail A, Hassan SS, Ramez AM. Therapeutic potency of ginger, garlic, and pomegranate extracts against cryptosporidium parvum-mediated gastro-splenic damage in mice. Acta Parasitol. 2023;68(1):32–41. https://doi.org/10.1007/s11686-022-00635-0 PMID: 36348178

98. Elfalleh W. Total phenolic contents and antioxidant activities of pomegranate peel, seed, leaf and flower. J Med Plants Res. 2012;6(32):. https://doi.org/10.5897/jmpr11.995

99. Weyl-Feinstein S, Markovics A, Eitam H, Orlov A, Yishay M, Agmon R, et al. Short communication: effect of pomegranate-residue supplement on Cryptosporidium parvum oocyst shedding in neonatal calves. J Dairy Sci. 2014;97(9):5800–5. https://doi.org/10.3168/jds.2013-7136 PMID: 24952772

100. El Ezz N, Khalil F, Shaapan R. Therapeutic effect of onion (Allium cepa) and cinnamon (Cinnamomum zeylanicum) oils on cryptosporidiosis in experimentally infected mice. Global Veterinaria. n.d.;7179–83.

101. Al-Khayri JM, Sahana GR, Nagella P, Joseph BV, Alessa FM, Al-Mssallem MQ. Flavonoids as potential anti-inflammatory molecules: a review. Molecules. 2022;27(9):2901. https://doi.org/10.3390/molecules27092901 PMID: 35566252

102. Ullah A, Munir S, Badshah SL, Khan N, Ghani L, Poulson BG, et al. Important flavonoids and their role as a therapeutic agent. Molecules. 2020;25(22):5243. https://doi.org/10.3390/molecules25225243 PMID: 33187049

103. Farzaei MH, Singh AK, Kumar R, Croley CR, Pandey AK, Coy-Barrera E, et al. Targeting inflammation by flavonoids: novel therapeutic strategy for metabolic disorders. Int J Mol Sci. 2019;20(19):4957. https://doi.org/10.3390/ijms20194957 PMID: 31597283

104. Lago JHG, Toledo-Arruda AC, Mernak M, Barrosa KH, Martins MA, Tibério IFLC, et al. Structure-activity association of flavonoids in lung diseases. Molecules. 2014;19(3):3570–95. https://doi.org/10.3390/molecules19033570 PMID: 24662074

105. Bildziukevich U, Wimmerová M, Wimmer Z. Saponins of selected triterpenoids as potential therapeutic agents: a review. Pharmaceuticals (Basel). 2023;16(3):386. https://doi.org/10.3390/ph16030386 PMID: 36986485

106. Elshamy A, Farrag A-R, Mohamed S, Ali N, Mohamed T, Menshawy M, et al. Gastroprotective effects of ursolic acid isolated from Ochrosia elliptica on ethanol-induced gastric ulcer in rats. Med Chem Res. 2020;29113–25.